

# Active control of three-phase CNT/resin/fiber piezoelectric polymeric nanocomposite porous sandwich microbeam based on sinusoidal shear deformation theory

B. Roustavi Navi<sup>1</sup>, M. Mohammadimehr\*<sup>1</sup> and A. Ghorbanpour Arani<sup>1,2</sup>

<sup>1</sup> Department of Solid Mechanics, Faculty of Mechanical Engineering, University of Kashan, Kashan, Iran

<sup>2</sup> Institute of Nanoscience & Nanotechnology, University of Kashan, Kashan, Iran

(Received April 14, 2019, Revised August 3, 2019, Accepted September 3, 2019)

**Abstract.** Vibration control in mechanical equipments is an important problem where unwanted vibrations are vanish or at least diminished. In this paper, free vibration active control of the porous sandwich piezoelectric polymeric nanocomposite microbeam with microsensor and microactuator layers are investigated. The aim of this research is to reduce amplitude of vibration in micro beam based on linear quadratic regulator (LQR). Modified couple stress theory (MCST) according to sinusoidal shear deformation theory is presented. The porous sandwich microbeam is rested on elastic foundation. The core and face sheet are made of porous and three-phase carbon nanotubes/resin/fiber nanocomposite materials. The equations of motion are extracted by Hamilton's principle and then Navier's type solution are employed for solving them. The governing equations of motion are written in space state form and linear quadratic regulator (LQR) is used for active control approach. The various parameters are conducted to investigate on the frequency response function (FRF) of the sandwich microbeam for vibration active control. The results indicate that the higher length scale to the thickness, the face sheet thickness to total thickness and the considering microsensor and microactuator significantly affect LQR and uncontrolled FRF. Also, the porosity coefficient increasing, Skempton coefficient and Winkler spring constant shift the frequency response to higher frequencies. The obtained results can be useful for micro-electro-mechanical (MEMS) and nano-electro-mechanical (NEMS) systems.

**Keywords:** active control; porous and polymeric materials; piezoelectric sandwich microbeam; free vibration; sinusoidal shear deformation theory; surface stress effects

## 1. Introduction

Nowadays, the sandwich structures are very interesting in the engineering systems due to their light weight and the elevated flexural stiffness. For meeting of these properties, the sandwich structures consist of two thin face sheets and thicker core and they tolerate mechanical loads by existing two reinforced face sheet as the carbon nanotube (CNT) reinforced polymeric. The polymeric reinforced sandwich nanocomposite structures may be employed in the new advanced applications as: energy harvester (Akavci 2016, Zeng *et al.* 2017), sensor and actuator (Kolahchi *et al.* 2017, Noh *et al.* 2017), electronic (Park *et al.* 2016, Zhang *et al.* 2017, Zonghong *et al.* 2017), monitoring (Nath and Kapuria 2012), microwave absorber (Yang *et al.* 2013, Khurram *et al.* 2015), reflector (Choi *et al.* 2012), energy absorption (Wu *et al.* 2017), porous sandwich radio frequency antenna (Tummala *et al.* 2017), and dielectric radar domes (Alankaya 2017).

There are two types of structure controls: active and passive controls. In the passive control, the control is done based on structure properties but in active control, the

external controller controls the structure behavior. Different application of active control can be exemplified in various aspects such as: seismic protection (Bitaraf *et al.* 2010, Gudarzi and Zamanian 2013), improving boring bar performance (Klein and Nachtigal 2013), collecting pantograph (Collina *et al.* 2005), smart shape memory alloy composite flapper (Khana *et al.* 2018), plasma metamaterial (Uriri *et al.* 2018), ion transform in micro fluid (Park and Yossifon 2018), broadband plasmon induced transparency (Zhang *et al.* 2018a), cooling fan noise (Kent and Sommerfeldt 2004), noise and vibration (Kim and Yoon 2018, Yang *et al.* 2018a).

The free vibration of sandwich beam with piezoelectric layers considering transverse flexibility using finite element method was carried out by Beheshti-Aval and Lezgy-Nazargah (2012). Arani *et al.* (2011) presented dynamic stability of the double-walled carbon nanotube under axial loading embedded in an elastic medium by the energy method. Vibration control of functionally graded sandwich plate integrated with the patches of active constrained layer damping (ACLD) treatment was done by Kumar and Ray (2016). They concluded that the ACLD patches considerably progress the damping characteristics of the FG sandwich plates for restraining their vibrations. Also, the active damped vibration for sandwich beam was investigated by Ghosh *et al.* (2015). The embedding piezoelectric sensors were used in the sandwich structures

\*Corresponding author, Associate Professor,  
E-mail: mmohammadimehr@kashanu.ac.ir

by Konka *et al.* (2012) and Masmoudi *et al.* (2015).

High-order free vibration of three-layered symmetric sandwich beam using dynamic stiffness method was investigated by Damanpack and Khalili (2012). Mohammadimehr *et al.* (2015b) considered surface stress effect on the nonlocal biaxial buckling and bending analysis of polymeric piezoelectric nanoplate reinforced by CNT using eshelby-mori-tanaka approach. Free vibration analysis of soft-core sandwich panels with general boundary conditions was performed by Wang and Liang (2017). Study on low frequency energy harvesting system in laminated aluminum beam structures with delamination was done by Rao *et al.* (2018). Effect of agglomeration on the natural frequencies of functionally graded carbon nanotube-reinforced laminated composite doubly-curved shells was established by Tornabene *et al.* (2016). They illustrated that reinforcing phase significantly affects the dynamic characterization. In another work, they (2018a) proposed higher-order equivalent single layer theory for functionally graded free-form and doubly-curved sandwich shells. Design and analysis of piezoelectric smart beam for active vibration control using proportional integral derivative controller (PID) and pole placement technique were carried out by Chhabra *et al.* (2012). They employed Euler-Bernoulli beam theory, finite element method (FEM) and the state space techniques. They illustrated that the sufficient vibration control can be attained by the proposed method. Simulation of active vibration control of a cantilever beam using linear quadratic regulator (LQR), linear quadratic Gaussian (LQG) and  $H_\infty$  optimal controllers was presented by Khot and Khan (2015). They proved that  $H_\infty$  controller has the excellent close loop dynamic performance than LQR and LQG controller. A feedback vibration control system for vibration of magnetostrictive plate subjected to follower force using sinusoidal shear deformation theory was presented by Ghorbanpour Arani and Khoddami Maraghi (2015). They showed that magneto-mechanical coupling in magnetostrictive plate (MSP) act such as electro-hydraulic actuator, wireless linear Motors and sensors in control vibration behaviors of systems. The low-stiffness and high-stiffness actuator for two different vibration modes: out-of-plane and in-plane bending and extensional modes were made by Toledo *et al.* (2017). They found that the low-stiffness actuator is more suitable for the modal in-plane application. Some researchers worked about size dependent effect (Houari *et al.* 2016), carbon nanotubes reinforced composite (Lakshminpathi and Vasudevan 2019, Mohammadimehr *et al.* 2018a) and multi-physical fields such as magneto-electro-elastic fields (Mohammadimehr *et al.* 2016c, 2018b, Arefi and Zenkour 2018 and Mohammadimehr and Shahedi 2016).

Experimental study of local and modal approaches to active vibration control of elastic systems was studied by Belyaev *et al.* (2017). Frequency methods of the automatic control theory were used to design stable control systems. They demonstrated that the local control systems have appropriate performance at the first and the second resonance frequency. Adaptive fuzzy sliding mode controller to diminishing of the rotating carbon nanotube

reinforced composite beam vibration was modeled by Rahmani (2018). Sapra *et al.* (2018) developed active vibration control of a beam instrumented with MWCNT/epoxy nanocomposite sensor and PZT-5H actuator. Modeling of hybrid vibration control for multilayer structures using solid-shell finite elements was presented by Kpeky *et al.* (2018). They found that nonlinear active control laws reduce the amplitudes of vibrations with significant frequency dependence.

Rojas and Carcaterra (2018) presented an approach to optimal semi-active control (Krotov's method) of vibration energy harvesting based on MEMS. Particular emphasis to piezoelectric, electromagnetic and capacitive circuits was done for novel MEMS-based device control of vibration energy harvesting. Performance of a graphite wafer-reinforced viscoelastic composite layer for active-passive damping of plate vibration was investigated by Kumar *et al.* (2018). Their results indicated significantly improved active-passive damping in the overall plate for the inclusions of graphite-wafers. Zhang *et al.* (2018b) investigated generalized-disturbance rejection control with proportional-integral (GDR-PI) for vibrational suppression of piezoelectric laminated flexible structures based on the refined state space model. Their excited piezoelectric laminated flexible smart beam simulations showed that better vibrational suppression performance is obtained by the GDR-PI control. Dynamic control of aluminum beams integrated with nanocomposite piezoelectric layers considering CNT agglomeration effects subjected to blast load using hyperbolic viscopiezo-elasticity theory was analyzed by Sharif Zarei *et al.* (2018). They concluded that reinforcing of the facesheets with 5% CNTs leads to 59% reduction in the dynamic deflection. Analytical model for flexural damping responses of carbon fiber reinforced plastics (CFRP) cantilever beams in the low-frequency vibration was performed by Yang *et al.* (2018b). They found that there are large errors in the prediction second-order natural frequency of CFRP beam based on specific damping capacity (SDC) as the cross-section deformation and longitudinal strain of the beam have not been considered. An integrated approach for active vibration control of composite shallow shells using constant gain velocity feedback (CGVF) and LQR based on based on efficient zigzag theory was employed by Rahman *et al.* (2018). They concluded that in comparison to CGVF controller, a better control in smaller time is obtained by LQR controller for the similar boundary conditions. Free vibration analysis of functionally graded conical, cylindrical shell and annular plate structures with a four-parameter power-law distribution was presented by Tornabene (2009).

Modeling and active vibration control analysis of lattice grid beam with piezoelectric fiber composite using a novel fractional order  $PD_\mu$  algorithm were carried out by Xie *et al.* (2018). They demonstrated that the fractional order  $PD_\mu$  control can decrease the vibration amplitude of the beam faster than the integer order PD algorithm. Mevada and Prajapati (2018) studied active vibration control of smart beam under parametric variations. Reddy's third-order shear deformation active-passive control of functionally graded sandwich plate and shell structures was performed by Moita

*et al.* (2018). They found that placing of the piezoelectric sensor and actuator layers on the top and bottom of the sandwich structure created an active damping control better than as they are embedded. Ma *et al.* (2018) investigated active vibration control of an axially moving cantilever structure using PZT actuator. They used proportional plus derivative (PD) or fuzzy algorithm to create a closed-loop feedback system. They illustrated that velocity and tip mass considerably have an effect on vibration characteristics. Active control of thermal buckling and vibration for a sandwich composite laminated plate with piezoelectric fiber reinforced composite actuator face sheets was developed by Li *et al.* (2018). They displayed that active thermal buckling control and the vibration control improve the stability of the structure. Mechanical buckling analysis of functionally graded power-based and carbon nanotubes-reinforced composite plates and composite plates were carried out by Zghal *et al.* (2018) and Raju *et al.* (2015). In another work, Frikha *et al.* (2018) analyzed dynamic analysis of functionally graded carbon nanotubes-reinforced plate and shell structures using a double directors finite shell elements. The modified first order shear deformation theory-based four nodes finite shell element for thermal buckling analysis of functionally graded plates and cylindrical shells was proposed by Trabelsi *et al.* (2019). Their proposed theory consists on assuming a parabolic distribution of the transverse shear strains across the shell thickness. The generalized differential quadrature (GDQ) method to study the dynamic behavior of functionally graded materials (FGMs) and laminated doubly curved shells and panels based on generalization of the Reissner–Mindlin theory is developed by Tornabene *et al.* (2018b). Guo *et al.* (2018) presented the active and passive vibration control of double-layer hourglass lattice truss structures. The velocity feedback control method was used as controllers on vibration suppressing of the sandwich structure. Karagiannis and Radisavljevic-Gajic (2018) studied sliding mode boundary control of an Euler-Bernoulli beam subject to disturbances. They found that the controller dampen the vibrations exponentially at an arbitrary rate. Low frequency dynamics of a smart system and its state feedback based active control were modeled by Kant and Parameswaran (2018). They designed state feedback controller based on pole placement technique to actively suppress the vibrations. Active vibration control of piezoelectric smart beams with radial basis function generated finite difference collocation method for both open-circuit and closed-circuit electrical boundary conditions was employed by Chuaqui *et al.* (2018). They concluded that increasing of the piezoelectric layer thickness for the constant gains applied to the control system has not a significant effect in minimizing or eliminating the vibration.

Botta and Toccaceli (2018) analyzed active control of torsional vibrations of piezoelectric plates. Active dynamic control of laminated FG-CNT reinforced composite plates integrated with piezoelectric layers was investigated by Nguyen-Quang *et al.* (2018). Their research revealed that velocity feedback control algorithm based on a closed loop for controlling displacement or oscillation time or even both

can be employed adequately for the vibration of the plates. An enhanced method to control the residual vibrations of a single-link flexible glass fabric reinforced epoxy-glass composite manipulator was obtained by Yavuz (2019). They demonstrated that the residual vibration amplitudes of the flexible composite manipulator are concealed with the proposed method up to 99% for all velocity inputs. He *et al.* (2018) employed piezoelectric self-sensing actuator for active vibration control of motorized spindle based on adaptive signal separation. They illustrated that the displacement signal and the vibration of the motorized spindle can be reduced efficiently through a linear quadratic Gaussian algorithm. Qin *et al.* (2019) presented structural behavior of the stiffened double-skin profiled composite walls under compression.

The vibration active control of the porous sandwich nanocomposite microbeam was not investigated in the researches. The sinusoidal shear deformation and modified couple stress theories are extended for porous sandwich microactuator-microsensor with three-phase carbon nanotubes/fiber/polymer piezoelectric polymeric nanocomposite face sheets. Surface stress effects are considered. The Navier's type solution is developed for the vibration active control of the porous sandwich nanocomposite microbeam. Effects of the porosity and elastic foundation on the vibration active control are inspected.

## 2. The structure motion formulation

Schematic of the porous sandwich nanocomposite piezoelectric polymeric microbeam is shown in Fig. 1. The micro structure is embedded in the elastic foundation including Winkler spring ( $k_W$ ) and shear layer ( $k_g$ ). There is a microsensor and a microactuator on the top and bottom of the micro sandwich beam for its vibration control, respectively. The micro sandwich beam includes the porous core and three phase reinforced nanocomposite face sheets (CNT/fiber/resin with polymeric matrix). The three phase material estimation can be defined as (Gibson 1994, Reddy 2004, Kim *et al.* 2009, Bhardwaj *et al.* 2013, Arani *et al.* 2016)

$$\begin{aligned} E_{11} &= V_F E_F + V_M E_M, \rho = V_F \rho_F + V_M \rho_M, E_{22} = \frac{E_M (1 + \xi_1 \eta_E V_F)}{1 - \eta_E V_F}, \\ G_{12} &= \frac{G_M (1 + \xi_2 \eta_G V_F)}{1 - \eta_G V_F}, \eta_E = \frac{E_F / E_M - 1}{E_F / E_M + \xi_1}, \eta_G = \frac{G_F / G_M - 1}{G_F / G_M + \xi_2} \\ E_M &= E_{RE} \left[ \frac{3(1 - \eta_L V_{NT})(1 - \eta_D V_{NT})(d_{NT} + 2l_{NT} \eta_L V_{NT}) + 5d_{NT} (2\eta_D V_{NT} + 1)}{8d_{NT} (1 - \eta_D V_{NT})} \right] \quad (1) \\ G_M &= \frac{E_M}{2(1 + \nu_{RE})}, \eta_L = \frac{4tE_{NT} - E_{RE}d_{NT}}{2(2tE_{NT} + E_{RE}l_{NT})}, \eta_D = \frac{4tE_{NT} - E_{RE}d_{NT}}{2(2tE_{NT} + E_{RE}d_{NT})} \\ V_{NT} &= \frac{w_{NT}}{w_{NT} + (\rho_{NT} / \rho_{RE}) - (\rho_{NT} / \rho_{RE})w_{NT}} \end{aligned}$$

where  $\nu_{12}$ ,  $G_{12}$ ,  $E_{11}$  and  $E_{22}$  denote Poisson's ratio, shear modulus, longitudinal and transversely elastic moduli of the nanocomposite face sheet, respectively. F and M indices denote fiber and matrix of the nanocomposite, respectively. RE and NT are used for resin epoxy and

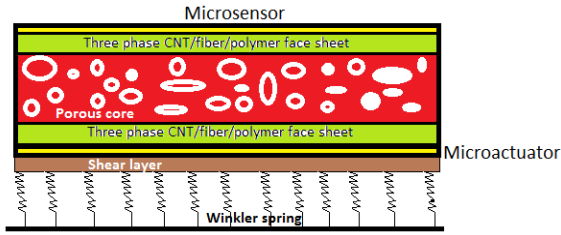


Fig. 1 A schematic view of the porous sandwich nanocomposite piezoelectric polymeric microbeam

nanotubes, respectively.  $E, \rho, w, V, d, l$  and  $t$  denote elastic modulus, density, mass fraction, volume fraction, diameter, length and thickness, respectively.  $\xi_1 = 2$  and  $\xi_2 = 1$  are supposed.

The volume fractions of top and bottom face sheets are considered as

$$\begin{aligned} V_{NT}^t &= 2 \left( \frac{z + h_c/2}{h_t} \right) V_{NT} \\ V_{NT}^b &= 2 \left( \frac{z - h_c/2}{h_t} \right) V_{NT} \end{aligned} \quad (2)$$

Sinusoidal shear deformation beam theory (SSDBT) for displacement field of the porous sandwich nanocomposite can be expressed as follows

$$\begin{aligned} u(x, z, t) &= u(x, t) + z\alpha + \frac{h}{\pi} \sin(\pi z/h) \left( \alpha + \frac{\partial w}{\partial x} \right) \\ w(x, z, t) &= w(x, t) \end{aligned} \quad (3)$$

where  $u$  and  $w$  are displacement along  $x$  and  $z$  directions.  $\alpha$  denotes the rotation about  $x$  direction.

The strains ( $\varepsilon_{ij}$ ), the stresses ( $\sigma_{ij}$ ) and the electrical displacements ( $D_i$ ) can be stated as follows

$$\begin{aligned} \varepsilon_{xx} &= \frac{\partial u}{\partial x} + f(z) \frac{\partial^2 w}{\partial x^2} + (f(z) + z) \frac{\partial \alpha}{\partial x}, \\ \varepsilon_{xz} &= \left( \frac{\partial f(z)}{2\partial z} + \frac{1}{2} \right) \left( \alpha + \frac{\partial w}{\partial x} \right) \end{aligned}$$

$$\begin{Bmatrix} \sigma_{xx}^Y \\ \sigma_{xz}^Y \\ D_x^X \\ D_z^X \end{Bmatrix} = \begin{bmatrix} Q_{11}^Y & 0 & 0 & e_{13}^X \\ 0 & Q_{55}^Y & 0 & 0 \\ 0 & e_{15}^X & \xi_{11}^X & 0 \\ e_{13}^X & 0 & 0 & \xi_{33}^X \end{bmatrix} \begin{Bmatrix} \varepsilon_{xx} \\ \varepsilon_{xz} \\ \varphi_{,x}^X \\ \varphi_{,z}^X \end{Bmatrix} \quad (4)$$

$$Q_{11}^c = (Q_{11}^c - \alpha_1^2 M),$$

$$M = \frac{(3G(z) - E(z))2G(z) + 3G(z)(E(z) - 2G(z))}{3(1 - \alpha B)(3G(z) - E(z))} B,$$

$$Q_{11}^i = \frac{E_{12}^i}{(1 - \nu_{12}^i \nu_{21}^i)}, \quad Q_{55}^i = G_{12}^i,$$

$$Y = b, t, c, s, a, X = s, a,$$

where  $Q_{ij}^k, e_{ij}^k$  and  $\xi_{ii}^k$  denote elastic, piezoelectric and dielectric constants.  $\alpha_1, M, B$  and  $\varphi$  denote Biot modulus, Biot, skempton coefficients and electrical potential function. The porous material types of sandwich core can be assumed as follows

Type A:

$$\begin{aligned} E(z) &= E \left[ 1 - e_0 \cos \left( \left( \frac{\pi}{2h_c} \right) \left( z + \frac{h_c}{2} \right) \right) \right] \\ G(z) &= G \left[ 1 - e_0 \cos \left( \left( \frac{\pi}{2h_c} \right) \left( z + \frac{h_c}{2} \right) \right) \right] \\ \rho(z) &= \rho \left[ 1 - e_m \cos \left( \left( \frac{\pi}{2h_c} \right) \left( z + \frac{h_c}{2} \right) \right) \right] \end{aligned} \quad (5a)$$

Type B:

$$\begin{aligned} E(z) &= E \left[ 1 - e_0 \cos \left( \frac{\pi z}{h_c} \right) \right] \\ G(z) &= G \left[ 1 - e_0 \cos \left( \frac{\pi z}{h_c} \right) \right] \\ \rho(z) &= \rho \left[ 1 - e_m \cos \left( \frac{\pi z}{h_c} \right) \right] \end{aligned} \quad (5b)$$

Type C:

$$\begin{aligned} E(z) &= E \left[ 1 - \left[ 1 - \left( \frac{2}{\pi} (1 - e_m) - \frac{2}{\pi} + 1 \right)^2 \right] \right] \\ G(z) &= G \left[ 1 - \left[ 1 - \left( \frac{2}{\pi} (1 - e_m) - \frac{2}{\pi} + 1 \right)^2 \right] \right] \\ \rho(z) &= \rho \sqrt{1 - \left[ 1 - \left( \frac{2}{\pi} (1 - e_m) - \frac{2}{\pi} + 1 \right)^2 \right]} \end{aligned} \quad (5c)$$

The porosity coefficients can be stated as  $e_0 = 1 - E_1/E$  or  $e_0 = 1 - G_1/G$  ( $0 \leq e_0 \leq 1$ ) and or  $e_m = 1 - \rho_1/\rho$  ( $0 \leq e_m \leq 1$ ).  $E, E_1, G, G_1, \rho$  and  $\rho_1$  denote minimum and maximum elastic moduli, shear moduli and densities of porous sandwich core.

The higher-order stresses ( $m_{ij}$ ) and rotations ( $\chi_{ij}$ ) of the microstructure based on modified couple stress and Eq. (3) can be obtained as follows (Mohammadimehr *et al.* 2016a)

$$\begin{aligned} m_{ij} &= 2Gl_2^2 \chi_{ij}, \chi_{ij} = \frac{1}{2} (\vartheta_{i,j} + \vartheta_{j,i}), \vartheta = \frac{1}{2} \text{curl}(u), \\ \vartheta_y &= \frac{1}{2} \left( \left[ \frac{\partial f(z)}{\partial z} + 1 \right] \alpha + \left[ \frac{\partial f(z)}{\partial z} - 1 \right] \frac{\partial w}{\partial x} \right) \\ \chi_{xy} &= \frac{1}{4} \left( \left[ -1 + \frac{\partial f(z)}{\partial z} \right] \frac{\partial^2 w}{\partial x^2} + \left[ 1 + \frac{\partial f(z)}{\partial z} \right] \frac{\partial \alpha}{\partial x} \right), \\ \chi_{yz} &= \frac{1}{4} \left( \frac{\partial^2 f(z)}{\partial z^2} \frac{\partial w}{\partial x} + \frac{\partial^2 f(z)}{\partial z^2} \alpha \right) \end{aligned} \quad (6)$$

where  $l_2$  is the length scale parameter.

Hamilton principle in the variation form can be expressed as follows

$$\int_{t_1}^{t_2} (\delta U - \delta K + \delta V) dt = 0 \quad (7)$$

where  $\delta K, \delta U$  and  $\delta V$  are kinetic energy, internal energy and external work variations, these variations with considering the surface stress effect can be derived as (Damanpack and Khalili 2012, Mohammadimehr *et al.*

2015a, 2017)

$$\delta K = \int_V \rho \left( \frac{\partial u}{\partial t} \frac{\partial \delta u}{\partial t} + \frac{\partial w}{\partial t} \frac{\partial \delta w}{\partial t} \right) dV + \int_A \rho_s \left( \frac{\partial u}{\partial t} \frac{\partial \delta u}{\partial t} + \frac{\partial w}{\partial t} \frac{\partial \delta w}{\partial t} \right) dA$$

$$= \int_V \left( \begin{aligned} & \left[ -f(z) \frac{\partial^3 w}{\partial x \partial t^2} - \frac{\partial^2 u}{\partial t^2} - (f(z) + z) \frac{\partial^2 \alpha}{\partial t^2} \right] \delta u \\ & + \left[ \begin{aligned} & -f(z)(f(z) + z) \frac{\partial^3 w}{\partial x \partial t^2} \\ & - (f(z) + z) \frac{\partial^2 u}{\partial t^2} - (f(z) + z)^2 \frac{\partial^2 \alpha}{\partial t^2} \end{aligned} \right] \delta \alpha \\ & + \left[ \begin{aligned} & f^2(z) \frac{\partial^4 w}{\partial x^2 \partial t^2} + f(z) \frac{\partial^3 u}{\partial t^2 \partial x} \\ & + f(z)(f(z) + z) \frac{\partial^3 \alpha}{\partial x \partial t^2} - \frac{\partial^2 w}{\partial t^2} \end{aligned} \right] \delta w \end{aligned} \right) \rho dz dA \tag{8}$$

$$+ \int_A \rho_s \left( \begin{aligned} & \left[ -(b+h) \frac{\partial^2 u}{\partial t^2} \right] \delta u \\ & + \left[ -\sin\left(\frac{2b}{h}\right) \frac{\partial^2 \alpha}{2 \partial t^2} - \left(\frac{bh^2}{2} + \frac{h^3}{6}\right) \frac{\partial^2 \alpha}{\partial t^2} \right] \delta \alpha \\ & + \left[ -(b+h) \frac{\partial^2 w}{\partial t^2} + \sin\left(\frac{2b}{h}\right) \frac{\partial^3 w}{\partial x \partial t^2} \right] \delta w \end{aligned} \right) dA$$

$$\rho = \rho^c + \rho^t + \rho^b + \rho^a + \rho^s$$

$$+ E_s \left( \frac{bh^2}{2} + \frac{h^3}{6} + p_1 \right) \left( \frac{\partial^4 w}{\partial x^4} \right) \delta w$$

$$+ \tau_s (b + h + p_4) \left( \frac{\partial w}{\partial x} \right) \delta \alpha - \tau_s (b + h + p_4) \left( \frac{\partial \alpha}{\partial x} \right) \delta w$$

$$p_1 = E_s \left( \frac{h}{2} - \frac{h}{2\pi} \right) \sin\left(\frac{\pi b}{h}\right)$$

$$p_2 = \frac{-2h}{\pi} E_s - E_s \left( \frac{h}{2} - \frac{h}{2\pi} \right) \sin\left(\frac{\pi b}{h}\right)$$

$$p_3 = \frac{-2h}{\pi} E_s - E_s \left( \frac{h}{2} - \frac{h}{2\pi} \right) \sin\left(\frac{\pi b}{h}\right) - 2E_s (bh^2/2 + h^3/6)$$

$$p_4 = \sin\left(\frac{\pi b}{h}\right) + \cos\left(\frac{\pi b}{h}\right) \tag{9}$$

$$\delta V = \int_A (k_w w - k_g \nabla^2 w + f) \delta w dA \tag{10}$$

The electrical functions for microsensor (indexed by s) and microactuator (indexed by a) can be expressed as

$$\varphi^a(x, z, t) = \frac{2z}{h_a} V(x, t) + \left( z^2 - \left(\frac{h_a}{2}\right)^2 \right) \varphi_0^a(x, t)$$

$$\varphi^s(x, z, t) = \left( z^2 - \left(\frac{h_s}{2}\right)^2 \right) \varphi_0^s(x, t) \tag{11}$$

By substituting Eqs. (8), (9) and (10) into Eq. (7), the motion equations of the porous sandwich nanocomposite microbeam can be obtained as

$$\delta U = \int_V \left( \begin{aligned} & \sum_{k=a,b,c,t,s} \sigma_{xx}^k \delta \varepsilon_{xx} + 2\sigma_{xz}^k \delta \varepsilon_{xz} \\ & + 2m_{xy} \delta \chi_{xy} + 2m_{yz} \delta \chi_{yz} \\ & + \sum_{k=s,a} D_z^k \frac{\partial \delta \varphi^k}{\partial z} + D_x^k \frac{\partial \delta \varphi^k}{\partial x} \end{aligned} \right) dV$$

$$+ \int_A (\sigma_x^s \delta \varepsilon_x + \sigma_y^s \delta \varepsilon_y + \sigma_{xz}^s \delta \varepsilon_{xz} + \sigma_{yz}^s \delta \varepsilon_{yz}) dA$$

$$\delta U = \int_V \left( \begin{aligned} & \left[ -\frac{\partial}{\partial x} (\sigma_{xx}^k) \right] \delta u + \left[ -\frac{\partial}{\partial x} (f(z) + z) \sigma_{xx}^k \right] \delta \alpha \\ & + \sigma_{xz}^k \left( \frac{\partial f(z)}{\partial z} + 1 \right) \delta \alpha \\ & + \frac{\partial^2}{\partial x^2} \left( \left[ \frac{\partial f(z)}{\partial z} - 1 \right] \frac{m_{xy}}{2} \right) \delta w \\ & + \frac{\partial}{\partial x} \left( \frac{m_{xy}}{2} \left[ \frac{\partial f(z)}{\partial z} + 1 \right] \right) \delta \alpha \\ & + \frac{\partial}{\partial x} \left( \frac{m_{yz}}{2} \frac{\partial^2 f(z)}{\partial z^2} \right) \delta w + \frac{\partial^2 f(z)}{\partial z^2} \frac{m_{yz}}{2} \delta \alpha \\ & + \left[ \frac{\partial^2}{\partial x^2} (f(z) \sigma_{xx}^k) - \frac{\partial}{\partial x} \left( \left( \frac{\partial f(z)}{\partial z} + 1 \right) \sigma_{xz}^k \right) \right] \delta w \\ & + \sum_{k=s,a} \left[ -\frac{\pi D_z^k \sin\left(\frac{\pi z}{h^k}\right)}{h^k} \delta \varphi^k - \frac{\partial}{\partial x} \left( D_x^k \cos\left(\frac{\pi z}{h^k}\right) \right) \delta \varphi^k \right] \end{aligned} \right) dV \tag{9}$$

$$\frac{v \tau_s h^2}{6(1-v)} \left( \frac{\partial^4 w}{\partial x^4} \right) \delta w$$

$$- p_3 \frac{\partial^2 \alpha}{\partial x^2} \delta \alpha - p_2 \frac{\partial^3 w}{\partial x^3} \delta \alpha + p_2 \frac{\partial^3 \alpha}{\partial x^3} \delta w$$

$$- \tau_s (b + h + p_4) \left( \frac{\partial^2 w}{\partial x^2} \right) \delta w$$

$$\delta u:$$

$$-\frac{\partial}{\partial x} (\sigma_{xx}^k) + f(z) \rho \frac{\partial^3 w}{\partial x \partial t^2} + \rho \frac{\partial^2 u}{\partial t^2} + \rho_s (b + h) \frac{\partial^2 u}{\partial t^2} + \rho a_1 \frac{\partial^2 \alpha}{\partial t^2} = 0$$

$$\delta \alpha^k:$$

$$-\frac{\partial}{\partial x} (a_1 \sigma_{xx}^k) + \sigma_{xz}^k \left( \frac{\partial f(z)}{\partial z} + 1 \right) - \frac{\partial}{\partial x} \left( \frac{m_{xy}}{2} \left( \frac{\partial f(z)}{\partial z} + 1 \right) \right) \delta \alpha + \frac{\partial^2 f(z)}{\partial z^2} \frac{m_{yz}}{2} + b_1 \rho \frac{\partial^3 w}{\partial x \partial t^2} + a_1 \rho \frac{\partial^2 u}{\partial t^2} + a_1^2 \rho \frac{\partial^2 \alpha}{\partial t^2} + \left[ -\frac{1}{2} \sin\left(\frac{2b}{h}\right) - \left(\frac{bh^2}{2} + \frac{h^3}{6}\right) \right] \frac{\partial^2 \alpha}{\partial t^2} - p_3 \frac{\partial^2 \alpha}{\partial x^2} - p_2 \frac{\partial^3 w}{\partial x^3} + \tau_s (b + h + p_4) \left( \frac{\partial w}{\partial x} \right) = 0 \tag{12}$$

$$\delta w:$$

$$\frac{\partial^2}{\partial x^2} (f(z) \sigma_{xx}^k) - \frac{\partial}{\partial x} \left( \left( \frac{\partial f(z)}{\partial z} + 1 \right) \sigma_{xz}^k \right) + \frac{\partial^2}{\partial x^2} \left( \left[ \frac{\partial f(z)}{\partial z} - 1 \right] \frac{m_{xy}}{2} \right) + \frac{\partial}{\partial x} \left( \frac{m_{yz}}{2} \frac{\partial^2 f(z)}{\partial z^2} \right) - f^2(z) \rho \frac{\partial^4 w}{\partial x^2 \partial t^2} - f(z) \rho \frac{\partial^3 u}{\partial t^2 \partial x} - b_1 \rho \frac{\partial^3 \alpha}{\partial x \partial t^2} + \rho \frac{\partial^2 w}{\partial t^2} + k_w w - k_g \nabla^2 w + \frac{v \tau_s h^2}{6(1-v)} \left( \frac{\partial^4 w}{\partial x^4} \right) \pm \tau_s (b + h + p_4) \left( \frac{\partial^2 w}{\partial x^2} \right)$$

$$\begin{aligned}
& +E_s \left( \frac{bh^2}{2} + \frac{h^3}{6} + p_1 \right) \left( \frac{\partial^4 w}{\partial x^4} \right) \\
& + p_2 \frac{\partial^3 \alpha}{\partial x^3} - \tau_s (b + h + p_4) \left( \frac{\partial \alpha}{\partial x} \right) = f \\
\delta \phi^a & - \frac{\pi D_z^a \sin\left(\frac{\pi z}{h^a}\right)}{h^a} - \frac{\partial}{\partial x} \left( D_x^a \cos\left(\frac{\pi z}{h^a}\right) \right) = 0 \\
\delta \phi^s & - \frac{\pi D_z^s \sin\left(\frac{\pi z}{h^s}\right)}{h^s} - \frac{\partial}{\partial x} \left( D_x^s \cos\left(\frac{\pi z}{h^s}\right) \right) = 0
\end{aligned} \tag{12}$$

By substituting Eqs. (1)-(6) into Eq. (12), the simplified motion equations can be derived as

$$\begin{aligned}
\delta u: \\
& -A_{11} \frac{\partial^2 u}{\partial x^2} - O_{11}^s \phi_{0,x}^s - O_{11}^a \phi_{,x}^a - O_{44}^a V_{,x} - C_{11} \frac{\partial^3 w}{\partial x^3} \\
& -B_{11} \frac{\partial^2 \alpha}{\partial x^2} + I_2 \frac{\partial^3 w}{\partial x \partial t^2} + I_0 \frac{\partial^2 u}{\partial t^2} + I_1 \frac{\partial^2 \alpha}{\partial t^2} \\
& + \rho_s (b + h) \frac{\partial^2 u}{\partial t^2} = 0 \\
\delta \alpha: \\
& -A_{22} \frac{\partial^2 u}{\partial x^2} - O_{22}^s \phi_{0,x}^s - O_{22}^a \phi_{0,x}^a - O_{55}^s V_{,x} \\
& -C_{22} \frac{\partial^3 w}{\partial x^3} - B_{22} \frac{\partial^2 \alpha}{\partial x^2} + A_{33} \alpha + A_{33} \frac{\partial w}{\partial x} + I_4 \frac{\partial^3 w}{\partial x \partial t^2} \\
& + G_{33} \frac{\partial w}{\partial x} + G_{33} \alpha + I_1 \frac{\partial^2 u}{\partial t^2} + I_3 \frac{\partial^2 \alpha}{\partial t^2} - G_{22} \frac{\partial^3 w}{\partial x^3} \\
& -G_{11} \frac{\partial^2 \alpha}{\partial x^2} + \left[ -\frac{1}{2} \sin\left(\frac{2b}{h}\right) - \left(\frac{bh^2}{2} + \frac{h^3}{6}\right) \right] \frac{\partial^2 \alpha}{\partial t^2} \\
& -p_3 \frac{\partial^2 \alpha}{\partial x^2} - p_2 \frac{\partial^3 w}{\partial x^3} + \tau_s (b + h + p_4) \left( \frac{\partial w}{\partial x} \right) = 0 \\
\delta w: \\
& C_{11} \frac{\partial^3 u}{\partial x^3} - O_{33}^s \phi_{0,xx}^s - O_{33}^a \phi_{0,xx}^a - O_{66}^a V_{,xx} \\
& + A_{44} \frac{\partial^4 w}{\partial x^4} + C_{22} \frac{\partial^3 \alpha}{\partial x^3} + I_3 \frac{\partial^4 w}{\partial x^2 \partial t^2} + I_2 \frac{\partial^2 u}{\partial t^2} - G_{33} \frac{\partial^2 w}{\partial x} \\
& -G_{33} \frac{\partial \alpha}{\partial x} + G_{44} \frac{\partial^4 w}{\partial x^4} - G_{22} \frac{\partial^3 \alpha}{\partial x^3} + I_4 \frac{\partial^2 \alpha}{\partial t^2} + I_0 \frac{\partial^2 w}{\partial t^2} \\
& + k_w w - k_g \nabla^2 w - A_{33} \frac{\partial \alpha}{\partial x} - A_{33} \frac{\partial^2 w}{\partial x^2} \\
& + \frac{\nu \tau_s h^2}{6(1-\nu)} \left( \frac{\partial^4 w}{\partial x^4} \right) - \tau_s (b + h + p_4) \left( \frac{\partial^2 w}{\partial x^2} \right) \\
& + E_s \left( \frac{bh^2}{2} + \frac{h^3}{6} + p_1 \right) \left( \frac{\partial^4 w}{\partial x^4} \right) + p_2 \frac{\partial^3 \alpha}{\partial x^3} \\
& - \tau_s (b + h + p_4) \left( \frac{\partial \alpha}{\partial x} \right) = f
\end{aligned} \tag{13}$$

$$\begin{aligned}
\delta \phi^a: \\
& -O_{11}^a \frac{\partial u}{\partial x} - (O_{22}^a + S_{11}^a) \frac{\partial \alpha}{\partial x} - (O_{33}^a + S_{11}^a) \frac{\partial^2 w}{\partial x^2} \\
& -Y_{33}^a V - Y_{11}^a \phi_0^a - Y_{22}^a V_{,xx} - Y_{44}^a \phi_{0,xx}^a = 0
\end{aligned}$$

$$\begin{aligned}
\delta \phi^s: \\
& -O_{11}^s \frac{\partial u}{\partial x} - (O_{22}^s + S_{11}^s) \frac{\partial \alpha}{\partial x} - (O_{33}^s + S_{11}^s) \frac{\partial^2 w}{\partial x^2} \\
& -R_{33}^s \phi_0^s - R_{11}^s \phi_{0,xx}^s = 0
\end{aligned}$$

The coefficients are presented in Appendix A.

### 3. Solving method and vibration active control of the micro structure

Navier's type solution for the simply supported porous sandwich piezoelectric nanocomposite microbeam is written as follows

$$\begin{aligned}
u(x, t) &= \sum_{m=1}^{\infty} u_m(t) \cos(m\pi x/L) \\
\alpha(x, t) &= \sum_{m=1}^{\infty} \alpha_m(t) \cos(m\pi x/L) \\
w(x, t) &= \sum_{m=1}^{\infty} w_m(t) \sin(m\pi x/L) \\
\phi^a(x, t) &= \sum_{m=1}^{\infty} \phi_m^a(t) \sin(m\pi x/L) \\
\phi^s(x, t) &= \sum_{m=1}^{\infty} \phi_m^s(t) \sin(m\pi x/L) \\
V(x, t) &= \sum_{m=1}^{\infty} V_m(t) \sin(m\pi x/L)
\end{aligned} \tag{14}$$

where  $m$  denotes the half axial wave numbers. The vibration active control equations in the space state using Eqs. (14) into Eqs. (13) can be obtained as

$$\begin{aligned}
M\ddot{d} + Kd &= DV(t) + fF_1(t), \quad d = [u, \alpha, w]^T, \\
K &= \begin{bmatrix} k_{11} & k_{12} & k_{13} \\ k_{21} & k_{22} & k_{23} \\ k_{31} & k_{32} & k_{33} \end{bmatrix}, \\
M &= \begin{bmatrix} I_0 + \rho_s(b+h) & & \\ & I_1 & \\ & & I_5 + \rho_s \left( \frac{bh^2}{2} + \frac{h^3}{6} \right) & \\ & & & vI_0 & \\ & & & & vI_4 & \\ & & & & & -v^2 I_3 + I_0 + \rho_s(b+h) \end{bmatrix}, \\
D &= \begin{bmatrix} -O_{11}^a Y_{33}^a v + O_{11}^a Y_{22}^a v^3 + vO_{44}^a \\ \frac{Y_{11}^a - Y_{44}^a v^2}{Y_{11}^a - Y_{44}^a v^2} \\ -O_{22}^a Y_{33}^a v + O_{22}^a Y_{22}^a v^3 + vO_{55}^s \\ \frac{Y_{11}^a - Y_{44}^a v^2}{Y_{11}^a - Y_{44}^a v^2} \\ -O_{33}^a Y_{33}^a v + O_{33}^a Y_{22}^a v^3 - O_{66}^a v^2 \\ \frac{Y_{11}^a - Y_{44}^a v^2}{Y_{11}^a - Y_{44}^a v^2} \end{bmatrix}, \\
f &= \begin{bmatrix} 0 \\ 0 \\ f_0 u(t) \end{bmatrix}, \\
k_{11} &= v^2 A_{11} - \frac{O_{11}^s O_{11}^s v^2}{R_{33}^s - R_{11}^s v^2} - \frac{O_{11}^a O_{11}^a v^2}{Y_{11}^a - Y_{44}^a v^2}, \\
k_{12} &= v^2 B_{11} - \frac{O_{11}^s (O_{22}^s + S_{11}^s) v^2}{R_{33}^s - R_{11}^s v^2} - \frac{O_{11}^a (O_{22}^a + S_{11}^a) v^2}{Y_{11}^a - Y_{44}^a v^2}, \\
k_{13} &= v^3 C_{11} - \frac{O_{11}^s (O_{33}^s + S_{11}^s) v^3}{R_{33}^s - R_{11}^s v^2} - \frac{O_{11}^a (O_{33}^a + S_{11}^a) v^3}{Y_{11}^a - Y_{44}^a v^2}, \\
k_{21} &= v^2 A_{22} - \frac{O_{22}^s O_{11}^s v^2}{R_{33}^s - R_{11}^s v^2} - \frac{O_{22}^a O_{11}^a v^2}{Y_{11}^a - Y_{44}^a v^2}, \\
k_{22} &= v^2 B_{22} - v^2 (-G_{11} - p_3) + G_{33} + A_{33}
\end{aligned} \tag{15}$$

$$\begin{aligned}
 k_{23} &= v^3 \frac{O_{22}^s(O_{22}^s + S_{11}^s)v^2}{R_{33}^s - R_{11}^s v^2} - \frac{O_{22}^a(O_{22}^a + S_{11}^a)v^2}{Y_{11}^a - Y_{44}^a v^2}, \\
 k_{31} &= v^3 \frac{O_{22}^s(O_{33}^s + S_{11}^s)v^3}{R_{33}^s - R_{11}^s v^2} - \frac{O_{22}^a(O_{33}^a + S_{11}^a)v^3}{Y_{11}^a - Y_{44}^a v^2} \\
 &\quad - v(-A_{33} - G_{33} + \tau_s(b + h + p_4)), \\
 k_{32} &= v^3 C_{11} - \frac{O_{33}^s O_{11}^s v^3}{R_{33}^s - R_{11}^s v^2} - \frac{O_{33}^a O_{11}^a v^3}{Y_{11}^a - Y_{44}^a v^2}, \\
 k_{33} &= v^3 (C_{22} + p_2 + G_{22}) \\
 &\quad + v(G_{33} + A_{33} + \tau_s(b + h + p_4)) \\
 &\quad - \frac{O_{33}^s(O_{22}^s + S_{11}^s)v^3}{R_{33}^s - R_{11}^s v^2} - \frac{O_{33}^a(O_{22}^a + S_{11}^a)v^3}{Y_{11}^a - Y_{44}^a v^2}, \\
 k_{33} &= v^4 \left( A_{44} + G_{44} + \frac{v\tau_s h^2}{6(1-v)} + \right. \\
 &\quad \left. \frac{E_s(bh^2/2 + h^3/6 + p_1)}{O_{33}^s(O_{33}^s + S_{11}^s)v^4} - \frac{O_{33}^a(O_{33}^a + S_{11}^a)v^4}{Y_{11}^a - Y_{44}^a v^2} \right) \\
 &\quad - \frac{O_{33}^s(O_{33}^s + S_{11}^s)v^4}{R_{33}^s - R_{11}^s v^2} - \frac{O_{33}^a(O_{33}^a + S_{11}^a)v^4}{Y_{11}^a - Y_{44}^a v^2} \\
 &\quad + v^2(G_{33} + A_{33} + \tau_s(b + h + p_4))
 \end{aligned} \tag{15}$$

$$\begin{aligned}
 P &= \begin{bmatrix} \dot{d} \\ \ddot{d} \end{bmatrix}, \dot{P} = \begin{bmatrix} \ddot{d} \\ \dddot{d} \end{bmatrix}, \ddot{d} = M^{-1}[DV - Kd], \\
 \dot{P} &= \begin{bmatrix} \ddot{d} \\ M^{-1}[DV - Kd] \end{bmatrix} \\
 \begin{bmatrix} \dot{d} \\ \ddot{d} \end{bmatrix} &= \begin{bmatrix} 0_{3 \times 3} & I_{3 \times 3} \\ -M^{-1}K & 0_{3 \times 3} \end{bmatrix} \begin{bmatrix} d \\ \dot{d} \end{bmatrix} + \begin{bmatrix} 0_{3 \times 3} \\ M^{-1}D \end{bmatrix} V \\
 \dot{P} &= AP + BV + B_1 f, X = CP \\
 A &= \begin{bmatrix} 0_{3 \times 3} & I_{3 \times 3} \\ -M^{-1}K & 0_{3 \times 3} \end{bmatrix}, \\
 B &= \begin{bmatrix} 0_{3 \times 3} \\ M^{-1}D \end{bmatrix}, B_1 = \begin{bmatrix} 0_{3 \times 3} \\ M^{-1}f \end{bmatrix}, \\
 C &= \begin{bmatrix} \cos\left(\frac{n\pi x}{l}\right) & 0 & 0 \\ 0 & \cos\left(\frac{n\pi x}{l}\right) & 0 \\ 0 & 0 & \sin\left(\frac{n\pi x}{l}\right) \end{bmatrix} 0_{3 \times 3}
 \end{aligned} \tag{16}$$

The block diagram of the vibration active control is illustrated in Fig. 2.

The linear quadratic regulator (LQR) is the effective and widely used linear control tool for determination of specific design and performance criteria. Here, LQR according to state space is used for controlling of free vibration of the sandwich structure. In this method, the actuator voltage obtains by optimum LQR solution control. The general LQR for can be stated as

$$J = \frac{1}{2} \int_0^\infty (P^T Q P + F^T R F) dt \tag{17}$$

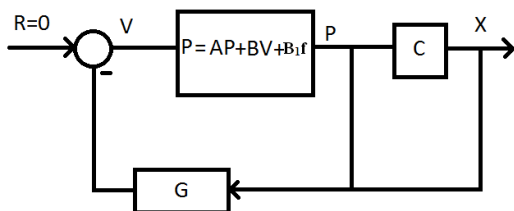


Fig. 2 The block diagram of vibration active control

where  $Q$  and  $R$  are the state weighting matrix and the control weighting matrix, respectively. The LQR problem search for a concession between minimum energy (control input) and best performance, hence

$$\begin{aligned}
 F &= -GP \\
 G &= R^{-1}B^T P
 \end{aligned} \tag{18}$$

$$\begin{aligned}
 F &= -GP \\
 G &= R^{-1}B^T P
 \end{aligned} \tag{19}$$

The solution reaches the Riccati equation

$$-PA - A^T P + PBR^{-1}B^T P - Q = 0 \tag{20}$$

The voltage of the actuator can be obtained as

$$V_{actuator} = B^{-1}GC V_{sensor} \tag{21}$$

#### 4. Numerical results and discussion

For the comparison, the obtained results and other literature results for different natural frequencies of simply supported microbeam are presented in Table 1. Damanpack and Khalili (2012) employed the first order shear deformation theory and higher order shear deformation theory for face sheets and core of sandwich microbeam. They used dynamic stiffness method and exact solution for calculating of the natural frequencies. Yang and Qiao (2005) considered dynamic effect of core with linear function in lateral direction in model B and both for lateral and axial direction for model C and without dynamic effect for core in model A. as it can be observed in this table, the present results based on sinusoidal shear deformation have a good agreement with the other results.

The dimension, elastic foundation and material properties of porous sandwich microactuator-microsensor with three-phase carbon nanotubes/fiber/polymer piezoelectric polymeric nanocomposite face sheets are listed as (Mohammadimehr *et al.* 2015a, Arani *et al.* 2016).

$$\begin{aligned}
 w_{NTs} &= 0.04, E_{PVDF} = 8.3GPa, v_{PVDF} = 0.18, \rho_{PVDF} = 1750kg / m^3 \\
 E_{resin} &= 2.72GPa, v_{resin} = 0.33, \rho_{resin} = 1200kg / m^3 \\
 E_{FG} &= 69GPa, v_{FG} = 0.2, \rho_{FG} = 1200kg / m^3, V_f = 0.55, \\
 E_c &= 2GPa, v_c = 0.3, \rho_c = 1020kg / m^3, e_0 = 0.5; B = 0, \\
 l_2 &= 17.6\mu m, e_{13} = -0.13, \xi_{11} = 1.1068e - 8, \\
 E_{NT} &= 400GPa, t_{NT} = 0.34nm, l_{NT} = 50\mu m, d_{NT} = 20nm, \rho_{NT} = 1350kg / m^3 \\
 h^s &= h^* = h / 10
 \end{aligned} \tag{22}$$

Fig. 3 displays present and Hamed and Rabinovitch (2009) results of dynamic deflection to static deflection ratio for simply supported beam under uniform step load. As it can be from this figure, the present results are matched to Hamed and Rabinovitch results. The time derivative equation has been solved by “ode45” in Matlab software. The time domain equation has been solved by Rung Kutta method.

Fig. 4 shows the displacement response of vibration active control and uncontrol of the porous sandwich carbon

Table 1 The natural frequencies of simply supported microbeam

Natural frequency	Exact (Damanpack and Khalili 2012)	DSM (Damanpack and Khalili 2012)	Model (A) (Yang and Qiao 2005)	Model (B) (Yang and Qiao 2005)	Model (C) (Yang and Qiao 2005)	ABAQUS (Yang and Qiao 2005)	Present work
$\omega_1$	2048.413	2048.413	2280.545	2050.769	2048.193	2198.235	2226.464
$\omega_2$	5189.672	5189.672	5771.106	5189.66	5183.377	4884.674	5520.170
$\omega_3$	8250.199	8250.199	9159.879	8180.546	8224.061	7673.089	8191.997

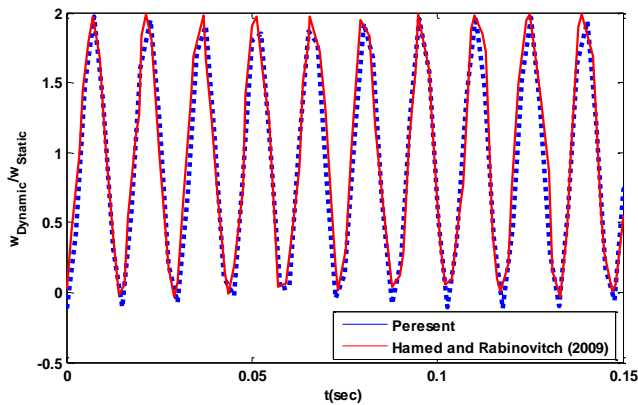


Fig. 3 Dynamic deflection to static deflection ratio for simply supported beam under uniform step load

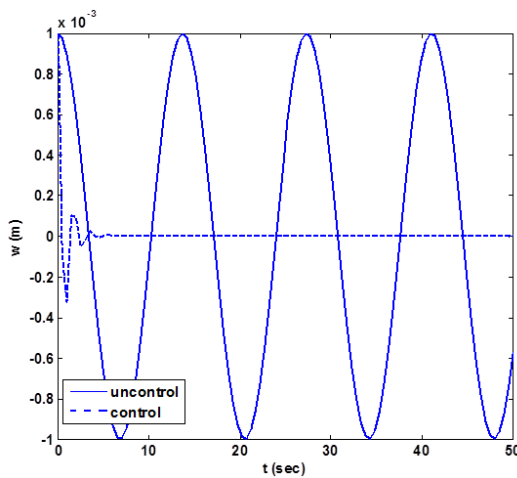


Fig. 4 The displacement response of vibration active control and uncontrol of the porous sandwich piezoelectric polymeric nanocomposite microbeam

nanotubes/fiber/polymer piezoelectric polymeric nanocomposite microbeam. As it is obvious that using LQR controller, the displacement is damped rapidly.

The frequency response of vibration active control and uncontrol of the porous sandwich piezoelectric polymeric nanocomposite microbeam is illustrated in Fig. 5. As the displacement figure, there is a dramatically cancellation in natural frequencies for LQR controller of the porous sandwich piezoelectric polymeric nanocomposite microbeam.

Fig. 6 displays the frequency response function of the porous sandwich piezoelectric polymeric nanocomposite

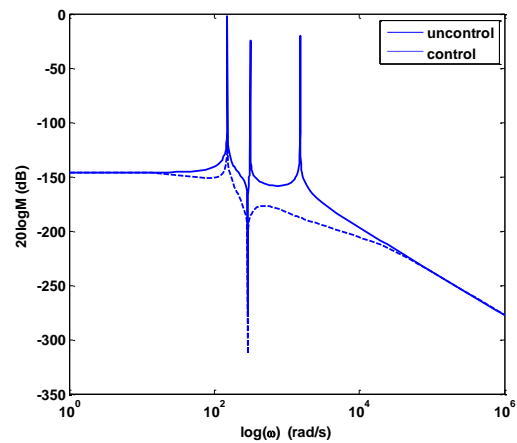


Fig. 5 The frequency response of vibration active control and uncontrol for the porous sandwich piezoelectric polymeric nanocomposite microbeam

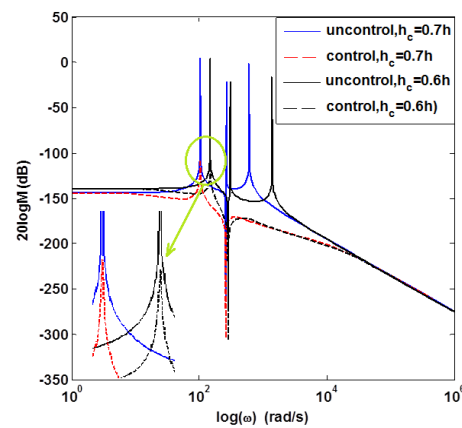


Fig. 6 The frequency response of the porous sandwich piezoelectric polymeric nanocomposite microbeam for different the core thickness to total thickness

microbeam for different the core thickness to total thickness. As it can be seen that with reduction in the core thickness to total thickness, the LQR has more reduction for FRF.

Fig. 7 shows the frequency response of the porous sandwich piezoelectric polymeric nanocomposite microbeam for different length scale to the total thickness ratio. As you can see that the higher length scale to the total thickness ratio leads to further reduction in the LQR controller.

The effect of Winkler spring and shear layer constants ( $k_w, k_g$ ) on the frequency response of the porous sandwich

piezoelectric polymeric nanocomposite microbeam is depicted in Figs. 8 and 9. In the uncontrol state, existence of Winkler foundation shifts the frequency response to higher frequencies. Also in the control state, the Winkler spring constant lessens the frequency response with shifting

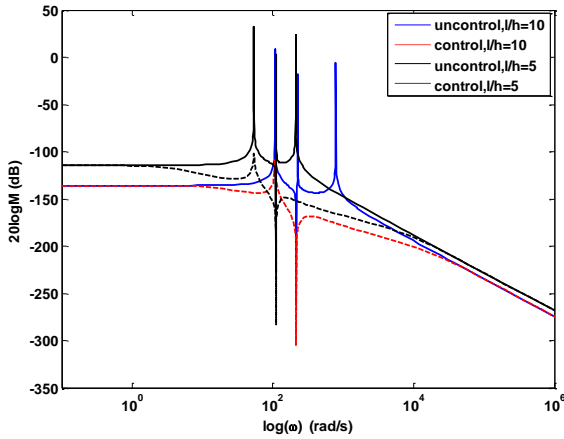


Fig. 7 The frequency response of the porous sandwich piezoelectric polymeric nanocomposite microbeam for different length scale to the total thickness ratio

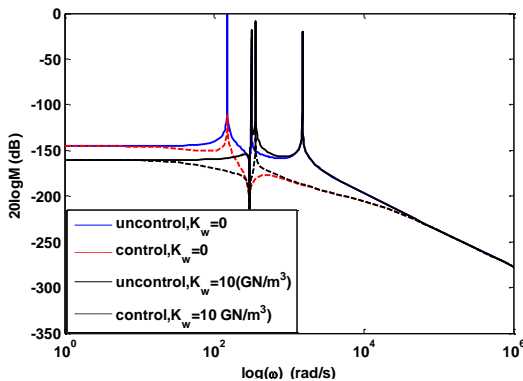


Fig. 8 The frequency response of the porous sandwich piezoelectric polymeric nanocomposite microbeam for different Winkler spring constant

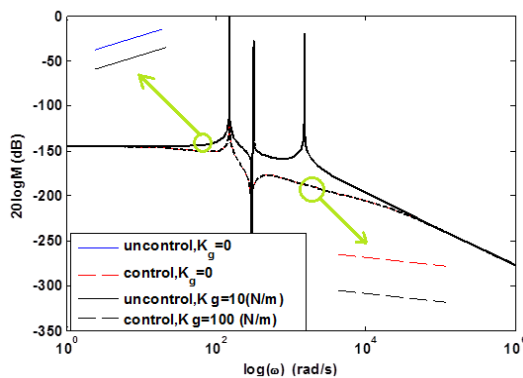


Fig. 9 The frequency response of the porous sandwich piezoelectric polymeric nanocomposite microbeam for different shear layer constant

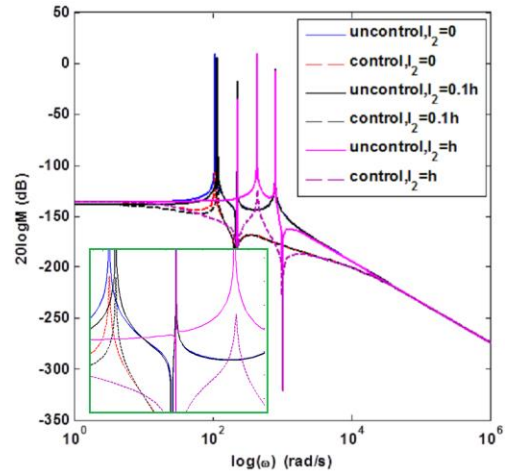


Fig. 10 Effect of the small scale parameter on the frequency response of the porous sandwich piezoelectric polymeric nanocomposite microbeam

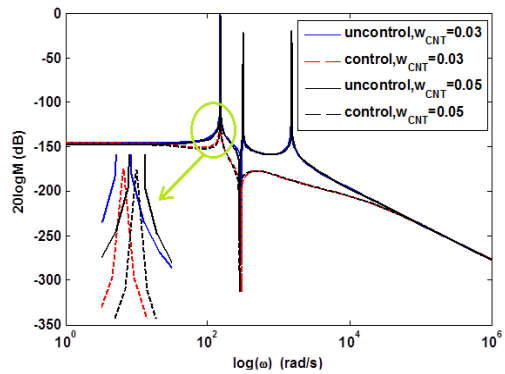


Fig. 11 Effect of the CNT weight fraction on the frequency response of the porous sandwich piezoelectric polymeric nanocomposite microbeam

of it. The FRF doesn't essentially influence by the shear layer constant.

Effect of the small scale to thickness ratio ( $l_2/h$ ) on the frequency response of the porous sandwich piezoelectric polymeric nanocomposite microbeam is illustrated in Fig. 10. As shown in Fig. 10, for the smaller small scale to thickness ratio, the FRF doesn't considerably changes but for the small scale value near to thickness ( $l_2 = h$ ), the FRF significantly reduces under LQR controller.

The effect of the CNT weight fraction ( $w_{CNT}$ ) on the frequency response of the porous sandwich piezoelectric polymeric nanocomposite microbeam is demonstrated in Fig. 11. In the uncontrolled state, the increasing the CNT weight fraction, decreases the FRF and moves it to higher frequency values but it doesn't affect LQR results.

Fig. 12 demonstrates effect of the microsensors/microactuator thickness ( $h_s, h_a$ ) on the frequency response of the porous sandwich piezoelectric polymeric nanocomposite microbeam. As it can be seen that the LQR FRF reduces and moves to higher frequency value.

Effects of the residual stress ( $\tau_s$ ), the Lamé ( $E_s$ ) and surface density ( $\rho_s$ ) constants on the frequency response of

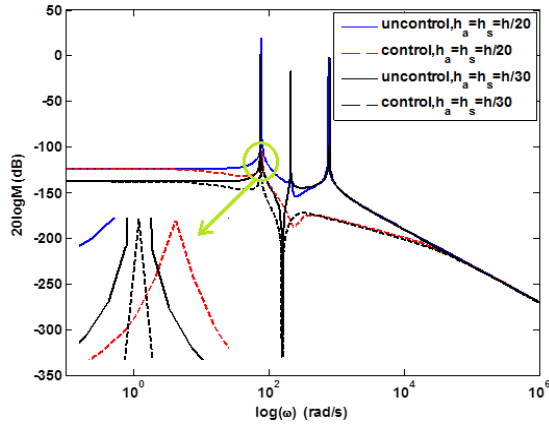


Fig. 12 Effect of the microsensor and micractorator thickness on the frequency response of the porous sandwich piezoelectric polymeric nanocomposite microbeam

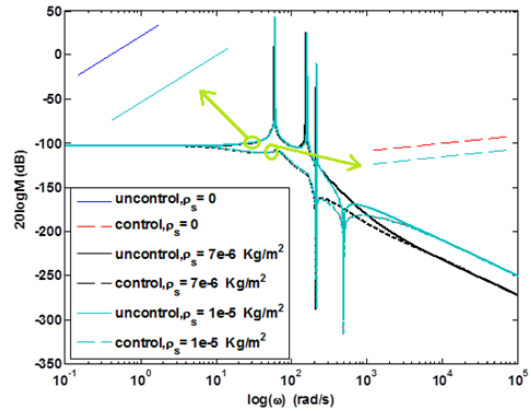


Fig. 15 Effect of the surface density constant on the frequency response of the porous sandwich piezoelectric polymeric nanocomposite microbeam

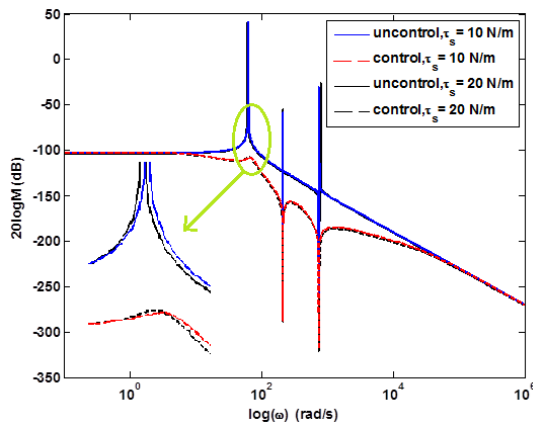


Fig. 13 Effect of the residual surface stress constant on the frequency response of the porous sandwich piezoelectric polymeric nanocomposite microbeam

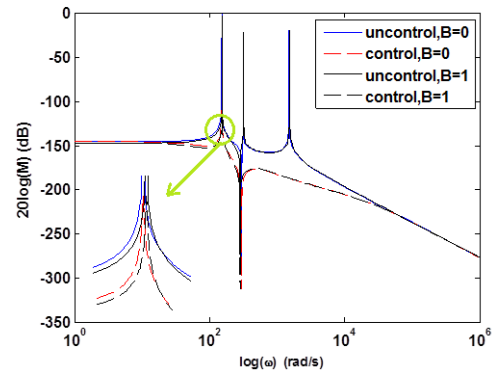


Fig. 16 Effect of Skempton coefficient on the frequency response of the porous sandwich piezoelectric polymeric nanocomposite microbeam

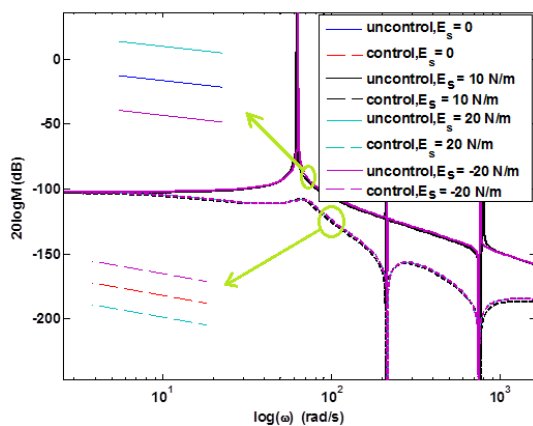


Fig. 14 Effect of the Lamé constant on the frequency response of the porous sandwich piezoelectric polymeric nanocomposite microbeam

the porous sandwich piezoelectric polymeric nanocomposite microbeam are shown in Figs. 13, 14 and 15. Among surface stress constant, the residual surface stress constant has higher effect on the FRF in uncontrol and control states. The Lamé and surface density doesn't have significant effects both on the LQR and uncontrol states of the structure.

Fig. 16 illustrates Skempton coefficient effect on the frequency response of the porous sandwich piezoelectric polymeric nanocomposite microbeam. Amplitude for both of the control and uncontrol states doesn't considerably change by considering Skempton coefficient.

The porosity effect on the frequency response of the porous sandwich piezoelectric polymeric nanocomposite microbeam are shown in Figs. 17 and 18 for three porosity type of A and B. It is clear that with increasing of the porosity coefficient, the FRF slowly moves to higher frequency.

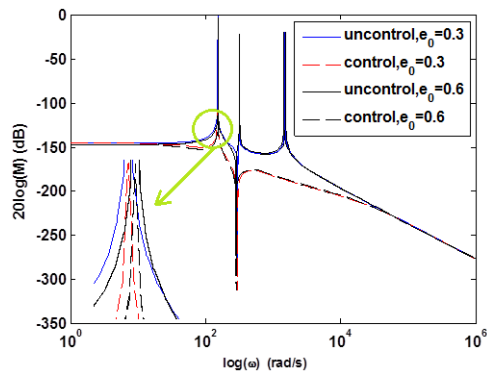


Fig. 17 Effect of the porosity coefficient (type A) on the frequency response of the porous sandwich piezoelectric polymeric nanocomposite microbeam

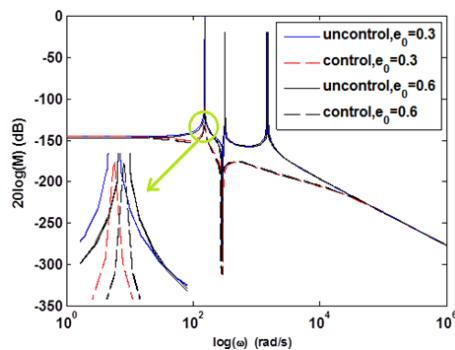


Fig. 18 Effect of the porosity coefficient (type B) on the frequency response of the porous sandwich piezoelectric polymeric nanocomposite microbeam

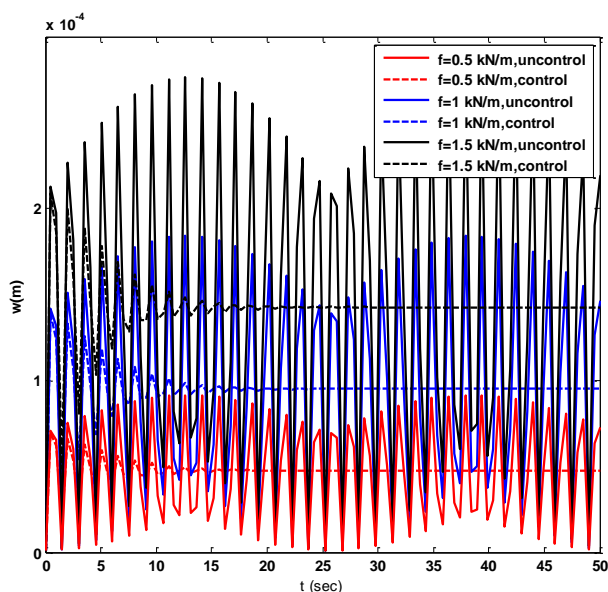


Fig. 19 Effect of step uniform load on the frequency response of the porous sandwich piezoelectric polymeric nanocomposite microbeam

The influence of step uniform load on the frequency response of the porous sandwich piezoelectric polymeric nanocomposite microbeam is shown in Fig. 19. It is seen that, in the control states, the higher load deflection is damped slower than smaller loads.

## 5. Conclusions

In this research, the free vibration active control of the porous sandwich piezoelectric polymeric nanocomposite microbeam was studied. Modified couple stress theory based on sinusoidal shear deformation theories were used. Surface stress effect was derived based on sinusoidal shear deformation theory. Three porous types were considered for sandwich core and CNT/fiber/polymer piezoelectric nanocomposite was extracted for face sheets. The porous sandwich microbeam was rested on elastic foundation. The LQR approach was used for controlling of the vibrational behavior. The following results can be obtained as follows:

- (1) LQR controller significantly reduces the vibrational amplitude of the porous sandwich piezoelectric polymeric nanocomposite microbeam.
- (2) The LQR controller effectively reduces FRF with raising of the face sheet thickness to total thickness.
- (3) LQR controller reduces considerably the FRF for higher length scale to the thickness.
- (4) Winkler spring constant has more effects on the LQR than the shear layer constant. The existence of Winkler spring constant shifts the frequency response to higher frequencies. The FRF doesn't essentially influence by the shear layer constant.
- (5) For the small scale value equal to the thickness, LQR controller reduces meaningfully.
- (6) FRF moves to higher frequency values with increasing of the CNT weight fraction.
- (7) The considering microsensor and microactuator with the sandwich nanocomposite microbeam has positive effect on the FRF both in control and uncontrol states.
- (8) The highest effects on the FRF for surface stress parameter is related to the residual surface stress constant.
- (9) Skempton coefficient shifts control and uncontrol FRF to higher frequencies.
- (10) The FRF moves slowly to higher frequency with the increasing porosity coefficient.

## Acknowledgments

The authors would like to thank the referees for their valuable comments. Also, they are thankful to the Iranian Nanotechnology Development Committee for their financial support, Iranian National Science Foundation (INSF) and the University of Kashan for supporting this work by Grant No. 682561/19.

## References

- Akavci, S.S. (2016), "Mechanical behavior of functionally graded sandwich plates on elastic foundation", *Compos. Part B: Eng.*, **96**, 136-152. <https://doi.org/10.1016/j.compositesb.2016.04.035>
- Alankaya, V. (2017), "Analytical study on the mechanical performance of composite sandwich shells for dielectric radar domes", *J. Sandw. Struct. Mater.*, **19**(1), 108-130. <https://doi.org/10.1177/1099636215613296>
- Arani, A.G., Hashemian, M., Loghman, A. and Mohammadimehr, M. (2011), "Study of dynamic stability of the double-walled carbon nanotube under axial loading embedded in an elastic medium by the energy method", *J. Appl. Mech. Tech. Phys.*, **52**(5), 815-824. <https://doi.org/10.1134/S0021894411050178>
- Arani, A.G., Haghparast, E. and Zarei, H.B.A. (2016), "Vibration of axially moving 3-phase CNTFPC plate resting on orthotropic foundation", *Struct. Eng. Mech., Int. J.*, **57**(1), 105-126. <https://doi.org/10.12989/sem.2016.57.1.105>
- Arefi, M. and Zenkour, A.M. (2018), "Size-dependent vibration and electro-magneto-elastic bending responses of sandwich piezomagnetic curved nanobeams", *Steel Compos. Struct., Int. J.*, **29**(5), 579-590. <https://doi.org/10.12989/scs.2018.29.5.579>
- Beheshti-Aval, S. and Lezgy-Nazargah, M. (2012), "A coupled refined high-order global-local theory and finite element model for static electromechanical response of smart multilayered/sandwich beams", *Arch. Appl. Mech.*, **82**(12), 1709-1752. <https://doi.org/10.1007/s00419-012-0621-9>
- Beheshti-Aval, S. and Lezgy-Nazargah, M. (2013), "Coupled refined layerwise theory for dynamic free and forced response of piezoelectric laminated composite and sandwich beams", *Meccanica*, **48**(6), 1479-1500. <https://doi.org/10.1007/s11012-012-9679-2>
- Belyaev, A.K., Fedotov, A.V., Irschik, H., Nader, M., Polyanskiy, V.A. and Smirnova, N.A. (2017), "Experimental study of local and modal approaches to active vibration control of elastic systems", *Struct. Control Health Monitor.*, **25**(2), 10-30. <https://doi.org/10.1002/stc.2105>
- Bhardwaj, G., Upadhyay, A.K. and Pandey, R. (2013), "Non-linear flexural and dynamic response of CNT reinforced laminated composite plates", *Compos. Part B.*, **45**, 89-100. <https://doi.org/10.1016/j.compositesb.2012.09.004>
- Bitaraf, M., Ozbulut, O.E., Hurlbauss, S. and Barroso, L. (2010), "Application of semi active control strategies for seismic protection of buildings with MR dampers", *Eng. Struct.*, **32**(10), 3040-3047. <https://doi.org/10.1016/j.engstruct.2010.05.023>
- Botta, F. and Toccaceli, F. (2018), "Piezoelectric plate's distribution for active control of torsional vibrations", *Actuators*, **7**(2), 23-40. <https://doi.org/10.3390/act7020023>
- Chhabra, D., Narwal, K. and Singh, P. (2012), "Design and analysis of piezoelectric smart beam for active vibration control", *Int. J. Adv. Res. Technol.*, **1**(1), 1-5.
- Choi, I., Kim, J.G., Seo, I.S. and Lee, D.G. (2012), "Radar absorbing sandwich construction composed of CNT, PMI foam and carbon/epoxy composite", *Compos. Struct.*, **94**(9), 3002-3008. <https://doi.org/10.1016/j.compstruct.2012.04.009>
- Collina, A., Facchinetti, A., Fossati, F. and Resta, F. (2005), "An application of active control to the collector of a high-speed pantograph: simulation and laboratory tests", *Proceedings of the 44th IEEE Conference on Decision and Control*.
- Chuaqui, T.R.C., Roque1, C.M.C. and Ribeiro, P. (2018), "Active vibration control of piezoelectric smart beams with radial basis function generated finite difference collocation method", *J. Intel. Mater. Syst. Struct.*, **29**(13), 2728-2743. <https://doi.org/10.1177/1045389X18778363>
- Damanpack, A.R. and Khalili, S.M.R. (2012), "High-order free vibration analysis of sandwich beams with a flexible core using dynamic stiffness method", *Compos. Struct.*, **94**, 1503-1514. <https://doi.org/10.1016/j.compstruct.2011.08.023>
- Frikha, A., Zghal, A. and Dammak, F. (2018), "Dynamic analysis of functionally graded carbon nanotubes-reinforced plate and shell structures using a double directors finite shell elementis", *Aerosp. Sci. Technol.*, **78**, 438-451. <https://doi.org/10.1016/j.ast.2018.04.048>
- Gibson, R.F. (1994), *Principles of Composite Material Mechanics*, New York, NY, USA, McGraw-Hill, Inc.
- Ghorbanpour Arani, A. and Khoddami Maraghi, Z. (2015), "A feedback control system for vibration of magnetostrictive plate subjected to follower force using sinusoidal shear deformation theory", *Ain Shams Eng. J.*, **7**(1), 361-369. <https://doi.org/10.1016/j.asej.2015.04.010>
- Ghorbanpour Arani, A., Zarei, B. and Haghparast, E. (2016), "Application of Halpin-Tsai method in modelling and sizedependent vibration analysis of CNTs/fiber/polymer composite microplates", *J. Comput. Appl. Mech.*, **47**, 42-52. <https://doi.org/10.22059/jcmech.2016.59254>
- Ghosh, S., Agrawal, S., Pradhan, A.K. and Pandit, M.K. (2015), "Performance of vertically reinforced 1-3 piezo composites for active damping of smart sandwich beams", *J. Sandw. Struct. Mater.*, **17**(3), 258-277. <https://doi.org/10.1177/1099636214565656>
- Gudarzi, M. and Zamanian, H. (2013), "Application of active vibration control for earthquake protection of multi structural buildings", *Int. J. Sci. Res. Know. (IJSRK)*, **1**(11), 502-513. <http://dx.doi.org/10.12983/ijrsk-2013-p502-513>
- Guo, Z.K., Yang, X.D. and Zhang, W. (2018), "Dynamic analysis, active and passive vibration control of double-layer hourglass lattice truss structures", *J. Sandw. Struct. Mater.*, 1-28. <https://doi.org/10.1177/1099636218784339>
- Hamed, E. and Rabinovitch, O. (2009), "Modeling and dynamics of sandwich beams with a viscoelastic soft core", *AIAA Journal*, **47**(9), 2194-2211. <https://doi.org/10.2514/1.41840>
- He, Y., Chen, X., Liu, Z. and Qin, Y. (2018), "Piezoelectric self-sensing actuator for active vibration control of motorized spindle based on adaptive signal separation", *Smart Mater. Struct.*, **27**, 065011-65022. <https://doi.org/10.1088/1361-665X/aabff4>
- Houari, A., Adda Bedia, E.A. and Tounsi, A. (2016), "Size-dependent mechanical behavior of functionally graded trigonometric shear deformable nanobeams including neutral surface position", *Steel Compos. Struct., Int. J.*, **20**(5), 963-981. <https://doi.org/10.12989/scs.2016.20.5.963>
- Kant, M. and Parameswaran, A.P. (2018), "Modeling of low frequency dynamics of a smart system and its state feedback based active control", *Mech. Syst. Sig. Proc.*, **99**, 774-789. <https://doi.org/10.1016/j.ymsp.2017.07.018>
- Karagiannis, D. and Radisavljevic-Gajic, V. (2018), "Siding mode boundary control of an Euler Bernoulli beam subject to disturbances", *J. Vib. Control*, **24**(6), 1109-1122. <https://doi.org/10.1109/TAC.2018.2793940>
- Kent, L.G. and Sommerfeldt, S.D. (2004), "Application of theoretical modeling to multichannel active control of cooling fan noise", *J. Acoust. Soc. America*, **115**, 228-240. <https://doi.org/10.1121/1.1631940>
- Khana, S., Saib, Y. and Prabu, M. (2018), "Active control of smart shape memory alloy composite flapper for aerodynamic applications", *Procedia Compos. Sci.*, **133**, 134-140. <https://doi.org/10.1016/j.procs.2018.07.017>
- Khot, S.M. and Khan, Y. (2015), "Simulation of active vibration control of a cantilever beam using LQR, LQG and H-∞ optimal controllers", *J. Vib. Anal. Measur. Control*, **3**(2), 134-151.
- Khurram, A.A., Rakha, S.A., Ali, N., Asim, M.T., Guorui, Z. and Munir, A. (2015), "Microwave absorbing properties of lightweight nanocomposite/honeycomb sandwich structures", *J. Nanotechnol. Eng.*, **6**(1), 110-117.

- <https://doi.org/10.1115/1.4031472>
- Kim, B. and Yoon, J.Y. (2018), "Modified LMS strategies using internal model control for active noise and vibration control systems", *Appl. Sci.*, **8**(6), 1007-1023.  
<https://doi.org/10.3390/app8061007>
- Kim, M., Park, Y. and Okoli, O.I. (2009), "Processing, characterization, and modeling of carbon nanotube-reinforced multiscale composites", *Compos. Sci. Technol.*, **69**, 335-342.  
<https://doi.org/10.1016/j.compscitech.2008.10.019>
- Klein, R.G. and Nachtigal, C.L. (2013), "The application of active control to improve boring bar performance", *J. Dyn. Syst. Meas. Control*, **97**(2), 179-183. <https://doi.org/10.1115/1.3426899>
- Konka, H.P., Wahab, M.A. and Lian, K. (2012), "On mechanical properties of composite sandwich structures with embedded piezoelectric fiber composite sensors", *J. Eng. Mater. Technol., Transactions of the ASME*, **134**(1), 349-361.  
<https://doi.org/10.1115/1.4005349>
- Kpeky, F., Abed-Meraim, F., Daya, E.M. and Samah, O.D. (2018), "Modeling of hybrid vibration control for multilayer structures using solid-shell finite elements", *Mech. Adv. Mater. Struct.*, **5**(12), 1033-1046.  
<https://doi.org/10.1080/15376494.2017.1365987>
- Kolahchi, R., Zarei, M.S., Hajmohammad, M.H. and Nouri, A. (2017), "Wave propagation of embedded viscoelastic FG-CNT-reinforced sandwich plates integrated with sensor and actuator based on refined zigzag theory", *Int. J. Mech. Sci.*, **130**, 534-545.  
<https://doi.org/10.1016/j.ijmecsci.2017.06.039>
- Kumar, R.S. and Ray, M.C. (2016), "Smart damping of geometrically nonlinear vibrations of functionally graded sandwich plates using 1-3 piezoelectric composites", *Mech. Adv. Mater. Struct.*, **23**(6), 652-669.  
<https://doi.org/10.1080/15376494.2015.1028692>
- Kumara, A., Pandaa, S., Kumarb, A. and Narsaria, V. (2018), "Performance of a graphite wafer-reinforced viscoelastic composite layer for active-passive damping of plate vibration", *Compos. Struct.*, **186**, 303-314.  
<https://doi.org/10.1016/j.compstruct.2017.12.019>
- Lakshmipathi, J. and Vasudevan, R. (2019), "Dynamic characterization of a CNT reinforced hybrid uniform and non-uniform composite plates", *Steel Compos. Struct., Int. J.*, **30**(1), 31-46. <https://doi.org/10.12989/scs.2019.30.1.031>
- Li, J., Li, F. and Narita, Y. (2018), "Active control of thermal buckling and vibration for a sandwich composite laminated plate with piezoelectric fiber reinforced composite actuator facesheets", *J. Sandw. Struct. Mater.*, **12**, 1-19.  
<https://doi.org/10.1177/1099636218783168>
- Ma, G., Xu, M., Zhang, S., Zhang, Y. and Liu, X. (2018), "Active vibration control of an axially moving cantilever structure using PZT actuator", *J. Aeronaut. Eng.*, **31**(5), 04018049.  
[https://doi.org/10.1061/\(ASCE\)AS.1943-5525.0000853](https://doi.org/10.1061/(ASCE)AS.1943-5525.0000853)
- Masmoudi, S., El Mahi, A. and Turki, S. (2015), "Use of piezoelectric as acoustic emission sensor for in situ monitoring of composite structures", *Compos. B. Eng.*, **80**, 307-320.  
<https://doi.org/10.1016/j.compositesb.2015.06.003>
- Mevada, J.R. and Prajapati, J.M. (2018), "Active vibration control of smart beam under parametric variations", *J. Brazil. Soc. Mech. Sci. Eng.*, **40**, 394-405.  
<https://doi.org/10.1007/s40430-018-1310-6>
- Mohammadimehr, M. and Shahedi, S. (2016), "Nonlinear magneto-electro-mechanical vibration analysis of double-bonded sandwich Timoshenko microbeams based on MSGT using GDQM", *Steel Compos. Struct., Int. J.*, **21**(1), 1-36.  
<https://doi.org/10.12989/scs.2016.21.1.001>
- Mohammadimehr, M., Rousta Navi, B. and Ghorbanpour Arani, A. (2015a), "Free vibration of viscoelastic double-bonded polymeric nanocomposite plates reinforced by FG-SWCNTs using MSGT, sinusoidal shear deformation theory and meshless method", *Compos. Struct.*, **131**, 654-671.  
<https://doi.org/10.1016/j.compstruct.2015.05.077>
- Mohammadimehr, M., Rousta Navi, B. and Ghorbanpour Arani, A. (2015b), "Surface stress effect on the nonlocal biaxial buckling and bending analysis of polymeric piezoelectric nanoplate reinforced by CNT using eshelby-mori-tanaka approach", *J. Solid Mech.*, **7**(2), 173-190.
- Mohammadimehr, M., Rousta Navi, B. and Ghorbanpour Arani, A. (2016a), "Modified strain gradient Reddy rectangular plate model for biaxial buckling and bending analysis of double-coupled piezoelectric polymeric nanocomposite reinforced by FG-SWNT", *Compos. Part B*, **87**, 132-148.  
<https://doi.org/10.1016/j.compositesb.2015.10.007>
- Mohammadimehr, M., Rostami, R. and Arefi, M. (2016b), "Electro-elastic analysis of a sandwich thick plate considering FG core and composite piezoelectric layers on Pasternak foundation using TSDT", *Steel Compos. Struct., Int. J.*, **20**(3), 513-544. <https://doi.org/10.12989/scs.2016.20.3.513>
- Mohammadimehr, M., Salemi, M. and Rousta Navi, B. (2016c), "Bending, buckling, and free vibration analysis of MSGT microcomposite Reddy plate reinforced by FG-SWCNTs with temperature-dependent material properties under hydro-thermo-mechanical loadings using DQM", *Compos. Struct.*, **138**, 361-380. <https://doi.org/10.1016/j.compstruct.2015.11.055>
- Mohammadimehr, M., Rousta Navi, B. and Ghorbanpour Arani, A. (2017), "Dynamic stability of MSGT sinusoidal viscoelastic piezoelectric polymeric FG-SWNT reinforced nanocomposite plate considering surface stress and agglomeration effects under hydro-thermo-electro-magneto-mechanical loadings", *Mech. Adv. Mater. Struct.*, **24**, 1325-1342.  
<https://doi.org/10.1080/15376494.2016.1227507>
- Mohammadimehr, M., Mohammadi-Dehabadi, A.A., Akhavan Alavi, S.M., Alambeigi, K., Bamdad, M., Yazdani, R. and Hanifehlo, S. (2018a) "Bending, buckling, and free vibration analyses of carbon nanotube reinforced composite beams and experimental tensile test to obtain the mechanical properties of nanocomposite", *Steel Compos. Struct., Int. J.*, **29**(3), 405-422.  
<https://doi.org/10.12989/scs.2018.29.3.405>
- Mohammadimehr, M., Mehrabi, M., Hadizadeh, H. and Hadizadeh, H. (2018b), "Surface and size dependent effects on static, buckling, and vibration of micro composite beam under thermo-magnetic fields based on strain gradient theory", *Steel Compos. Struct., Int. J.*, **26**(4), 513-531.  
<https://doi.org/10.12989/scs.2018.26.4.513>
- Moita, S.J., Araújo, L.A., Correia, V.F., Mota, C.M. and Herskovits, S.J. (2018), "Active-passive damping in functionally graded sandwich plate/shell structures", *Compos. Struct.*, **202**, 324-332.  
<https://doi.org/10.1016/j.compstruct.2018.01.089>
- Nath, J.K. and Kapuria, S. (2012), "Assessment of improved zigzag and smeared theories for smart cross-ply composite cylindrical shells including transverse normal extensibility under thermoelectric loading", *Arch. Appl. Mech.*, **82**(7), 859-877.  
<https://doi.org/10.1007/s00419-011-0597-x>
- Nguyen-Quang, K., Vo-Duy, T., Dang-Trung, H. and Nguyen-Thoi, T. (2018), "An isogeometric approach for dynamic response of laminated FG-CNT reinforced composite plates integrated with piezoelectric layers", *Comput. Methods Appl. Mech. Eng.*, **332**(15), 25-46.  
<https://doi.org/10.1016/j.cma.2017.12.010>
- Noh, M.S., Kim, S., Hwang, D.K. and Kang, C.Y. (2017), "Self-powered flexible touch sensors based on PZT thin films using laser lift-off", *Sensor Actuator Phys.*, **261**, 288-294.  
<https://doi.org/10.1016/j.sna.2017.04.046>
- Park, S. and Yossifon, G. (2018), "Electro-thermal based active control of ion transport in a microfluidic device with an ion-perm selective membrane", *Nanoscale*, **10**, 11633-11641.

- <https://doi.org/10.1039/C8NR02389A>
- Park, M., Lee, K.S., Shim, J., Liu, Y., Lee, C. and Cho, H. (2016), "Environment friendly, transparent nanofiber textiles consolidated with high efficiency PLEDs for wearable electronics", *Org. Electron.*, **36**, 89-96. <https://doi.org/10.1016/j.orgel.2016.05.030>
- Qin, Y., Li, Y.W., Lan, X.Z., Su, Y.S., Wang, X.Y. and Wu, Y.D. (2019), "Structural behavior of the stiffened double-skin profiled composite walls under compression", *Steel Compos. Struct., Int. J.*, **31**(1), 1-12. <https://doi.org/10.12989/scs.2019.31.1.001>
- Rahman, N., Alam, M.N. and Junaid, M. (2018), "Active vibration control of composite shallow shells: An integrated approach", *J. Mech. Eng. Sci.*, **12**(1), 3354-3369. <https://doi.org/10.15282/jmes.12.1.2018.6.0300>
- Rahmani, B. (2018), "Adaptive fuzzy sliding mode control for vibration suppression of a rotating carbon nanotube-reinforced composite beam", *J. Vib. Control*, **24**(2), 2447-2463. <https://doi.org/10.1177/1077546316687937>
- Raju, G., Wu, Z. and Weaver, P.M. (2015), "Buckling analysis of variable angle tow composite plates using differential quadrature method", *J. Indian Ins. Sci.*, **93**(4), 635-688.
- Reddy, J.N. (2004), *Mechanics of Laminated Composite Plates and Shells: Theory and Analysis*, (2<sup>nd</sup> ed.), New York, NY, USA, CRC Press.
- Rojas, A.R. and Carcaterra, A. (2018), "An approach to optimal semi-active control of vibration energy harvesting based on MEMS", *Mech. Syst. Sig. Proc.*, **107**, 291-316. <https://doi.org/10.1016/j.ymsp.2017.11.005>
- Rao Patange, S.S., Raja, S., Vijayakumar, M.P. and Ranganath, V.R. (2018), "Study on low frequency energy harvesting system in laminated aluminum beam structures with delamination", *J. Mech. Sci. Technol.*, **32**(5), 1985-1993. <https://doi.org/10.1007/s12206-018-0406-3>
- Sapra, G., Sharma, M. and Vig, R. (2018), "Active vibration control of a beam instrumented with MWCNT/epoxy nanocomposite sensor and PZT-5H actuator, robust to variations in temperature", *Microsyst. Technol.*, **24**(3), 1683-1694. <https://doi.org/10.1007/s00542-017-3551-1>
- Sharif Zarei, M., Hajmohammad, M.H., Kolahchi, R. and Karami, H. (2018), "Dynamic response control of aluminum beams integrated with nanocomposite piezoelectric layers subjected to blast load using hyperbolic viscopiezo-elasticity theory", *J. Sandw. Struct. Mater.*, 1-28. <https://doi.org/10.1177/1099636218785316>
- Toledo, J., Ruiz-Díez, V., Díaz, A., Ruiz, D., Donoso, A., Bellido, J.C., Wistrela, E., Kucera, M., Schmid, U., Hernando-García, J. and Sánchez-Rojas, J.L. (2017), "Design and characterization of in-plane piezoelectric microactuators", *Actuators*, **6**(2), 19-32. <https://doi.org/10.3390/act6020019>
- Tornabene, F. (2009), "Free vibration analysis of functionally graded conical, cylindrical shell and annular plate structures with a four-parameter power-law distribution", *Comput. Methods Appl. Mech. Eng.*, **198**(37-40), 2911-2935. <https://doi.org/10.1016/j.cma.2009.04.011>
- Tornabene, F., Fantuzzi, N., Bacciocchi, M. and Viola, E. (2016), "Effect of agglomeration on the natural frequencies of functionally graded carbon nanotube-reinforced laminated composite doubly-curved shells", *Compos. Part B*, **89**(1), 187-218. <https://doi.org/10.1016/j.compositesb.2015.11.016>
- Tornabene, F., Fantuzzi, N., Viola, E. and Batra, R.C. (2018a), "Stress and strain recovery for functionally graded free-form and doubly-curved sandwich shells using higher-order equivalent single layer theory", *Compos. Struct.*, **119**(1), 67-89. <https://doi.org/10.1016/j.compstruct.2014.08.005>
- Tornabene, F., Liverani, A. and Caligiana, G. (2018b), "FGM and laminated doubly curved shells and panels of revolution with a free-form meridian: A 2-D GDQ solution for free vibrations", *Int. J. Mech. Sci.*, **53**(6), 446-470. <https://doi.org/10.1016/j.ijmecsci.2011.03.007>
- Trabelsi, S., Frikha, A., Zghal, S. and Dammak, F. (2019), "A modified FSDT-based four nodes finite shell element for thermal buckling analysis of functionally graded plates and cylindrical shells", *Eng. Struct.*, **178**, 444-459. <https://doi.org/10.1016/j.engstruct.2018.10.047>
- Tummala, V.S., Mian, A., Chamok, N.H., Poduval, D., Ali, M. and Clifford, J. (2017), "Three dimensional printed dielectric substrates for radio frequency applications", *J. Electron. Packaging, Transactions of the ASME*, **139**(2), 020904. <https://doi.org/10.1115/1.4036384>
- Uriri, S.A., Tashima, T., Zhang, X., Asano, M., Bechu, M., Güney, D.Ö., Yamamoto, T., Özdemir, Ş.K., Wegener, M. and Tame, M.S. (2018), "Active control of a plasmonic metamaterial for quantum state engineering", *Phys. Rev. A*, **97**, 053810. <https://doi.org/10.1103/PhysRevA.97.053810>
- Wang, X. and Liang, X. (2017), "Free vibration of soft-core sandwich panels with general boundary conditions by harmonic quadrature element method", *Thin-Wall. Struct.*, **113**, 253-261. <https://doi.org/10.1016/j.tws.2016.12.004>
- Wu, Y., Liu, Q., Fu, J., Li, Q. and Hui, D. (2017), "Dynamic crash responses of bio-inspired aluminum honeycomb sandwich structures with CFRP panels", *Compos. B Eng.*, **121**, 122-133. <https://doi.org/10.1016/j.compositesb.2017.03.030>
- Xie, C., Wu, Y. and Liu, Z. (2018), "Modeling and active vibration control of lattice grid beam with piezoelectric fiber composite using fractional order PD $\mu$  algorithm", *Compos. Struct.*, **198**, 126-134. <https://doi.org/10.1016/j.compstruct.2018.05.060>
- Yang, M. and Qiao, P. (2005), "Higher-order impact modeling of sandwich structures with flexible core", *Int. J. Solids Struct.*, **42**, 5460-5490. <https://doi.org/10.1016/j.ijsolstr.2005.02.037>
- Yang, L., Fan, H., Liu, J., Ma, Y. and Zheng, Q. (2013), "Hybrid lattice-core sandwich composites designed for microwave absorption", *Mater. Des.*, **50**, 863-871. <https://doi.org/10.1016/j.matdes.2013.03.032>
- Yang, L., Liu, S., Zhang, H., Wu, H., Li, H. and Jiang, J. (2018a), "Hybrid Filtered-x adaptive vibration control with internal feedback and online identification", *Shock and Vib.*, 9010567. <https://doi.org/10.1155/2018/9010567>
- Yang, M., Hu, Y., Zhang, J., Ding, G. and Song, C. (2018b), "Analytical model for flexural damping responses of CFRP cantilever beams in the low-frequency vibration", *J. Low Freq. Noise Vib. Act. Control*, **37**(4), 669-681. <https://doi.org/10.1177/1461348418756024>
- Yavuz, Ş. (2019), "An enhanced method to control the residual vibrations of a single-link flexible glass fabric reinforced epoxy-glass composite manipulator", *Compos. Part B*, **159**(15), 405-417. <https://doi.org/10.1016/j.compositesb.2018.10.019>
- Zeng, Z., Gai, L., Petitpas, A., Li, Y., Luo, H. and Wang, D. (2017), "A flexible, sandwich structure piezoelectric energy harvester using PIN-PMN-PT/epoxy 2-2 composite flake for wearable application", *Sensor Actuator Phys.*, **265**, 62-69. <https://doi.org/10.1016/j.sna.2017.07.059>
- Zghal, A., Frikha, A. and Dammak, F. (2018), "Mechanical buckling analysis of functionally graded power-based and carbon nanotubes-reinforced composite plates and curved panels", *Compos. Part B*, **150**, 165-183. <https://doi.org/10.1016/j.compositesb.2018.05.037>
- Zhang, Y., Campbell, S.A., Zhang, L. and Karthikeyan, S. (2017), "Sandwich structure based on back-side etching silicon (100) wafers for flexible electronic technology", *Microsyst. Technol.*, **23**(3), 739-743. <https://doi.org/10.1007/s00542-015-2737-7>
- Zhang, Z., Yang, J., He, X., Han, Y., Zhang, J., Huang, J., Chen, D. and Xu, S. (2018a), "Active control of broadband plasmon-induced transparency in a terahertz hybrid metal-graphene metamaterial", *RSC Advances*, **8**, 27746-27753.

<https://doi.org/10.1039/C8RA04329A>

Zhang, X.Y., Wang, R.X., Zhang, S.Q., Wang, Z.X., Qin, X.S. and Schmidt, R. (2018b), "Generalized-disturbance rejection control for vibration suppression of piezoelectric laminated flexible structures", *Shock Vib.*, 1538936.

<https://doi.org/10.1155/2018/1538936>

Zonghong, X., Wei, Z., Peng, Z. and Xiang, L. (2017), "Design and development of conformal antennacomposite structure", *Smart Mater. Struct.*, 26(9), 095009.

<https://doi.org/10.1088/1361-665X/aa7918>

CC

## Appendix A

$$\begin{aligned}
 A_{11}^k &= \int_{-h^k/2}^{h^k/2} Q_{11}^k dz, B_{11}^k = \int_{-h^k/2}^{h^k/2} (f(z) + z) Q_{11}^k dz, C_{11}^k = \int_{-h^k/2}^{h^k/2} f(z) Q_{11}^k dz, \\
 A_{22}^k &= \int_{-h^k/2}^{h^k/2} (f(z) + z) Q_{11}^k dz, B_{22}^k = \int_{-h^k/2}^{h^k/2} (f(z) + z)^2 Q_{11}^k dz, C_{22}^k = \int_{-h^k/2}^{h^k/2} f(z)(f(z) + z) Q_{11}^k dz, \\
 A_{33}^k &= \int_{-h^k/2}^{h^k/2} \left( \frac{\partial f(z)}{\partial z} + 1 \right)^2 Q_{55}^k dz, A_{44}^k = \int_{-h^k/2}^{h^k/2} f^2(z) Q_{11}^k dz, \\
 D_{11}^c &= \int_{-h^k/2}^{h^k/2} \alpha_1^2 M dz, E_{11}^c = \int_{-h^k/2}^{h^k/2} (f(z) + z) \alpha_1^2 M dz, F_{11}^c = \int_{-h^k/2}^{h^k/2} f(z) \alpha_1^2 M dz, \\
 D_{22}^c &= \int_{-h^k/2}^{h^k/2} (f(z) + z) \alpha_1^2 M dz, E_{22}^c = \int_{-h^k/2}^{h^k/2} (f(z) + z)^2 \alpha_1^2 M dz, F_{22}^c = \int_{-h^k/2}^{h^k/2} f(z)(f(z) + z) \alpha_1^2 M dz, \\
 D_{33}^c &= \int_{-h^k/2}^{h^k/2} f(z) \alpha_1^2 M dz, O_{11}^k = \int_{-h^k/2}^{h^k/2} e_{13}^k 2z dz, O_{22}^k = \int_{-h^k/2}^{h^k/2} 2(f(z) + z) e_{13}^k z dz, O_{33}^k = \int_{-h^k/2}^{h^k/2} f(z) e_{13}^k 2z dz, \\
 S_{11}^k &= \int_{-h^k/2}^{h^k/2} \pi \cos(\pi z/h^a) / h^a \left( \frac{\partial f(z)}{\partial z} + \frac{1}{2} \right) e_{15}^k dz, R_{11}^k = \int_{-h^k/2}^{h^k/2} \xi_{11}^k \cos(\pi z/h^k) \left( z^2 - \left( \frac{h^k}{2} \right)^2 \right) dz \\
 , R_{33}^k &= \int_{-h^k/2}^{h^k/2} 2(\pi/h^k) z \xi_{33}^k \sin(\pi z/h^k) dz, O_{44}^k = \int_{-h^k/2}^{h^k/2} e_{13}^k dz/h^a, O_{55}^k = \int_{-h^k/2}^{h^k/2} (f(z) + z) e_{13}^k dz/h^a \\
 I_0^k &= \int_{-h^k/2}^{h^k/2} \rho^k dz, I_1^k = \int_{-h^k/2}^{h^k/2} (f(z) + z) \rho^k dz, I_2^k = \int_{-h^k/2}^{h^k/2} \rho^k f(z) dz, I_4^k = \int_{-h^k/2}^{h^k/2} \rho^k f(z)(f(z) + z) dz \\
 I_3^k &= \int_{-h^k/2}^{h^k/2} \rho^k f^2(z) dz, I_5^k = \int_{-h^k/2}^{h^k/2} \rho^k (f(z) + z)^2 dz, G_{11}^k = \int_{-h^k/2}^{h^k/2} \frac{1}{4} G l_2^2 \left( 1 + \frac{\partial f(z)}{\partial z} \right)^2 dz, \\
 G_{22}^k &= \int_{-h^k/2}^{h^k/2} \frac{1}{4} G l_2^2 \left( 1 + \frac{\partial f(z)}{\partial z} \right) \left( \frac{\partial f(z)}{\partial z} - 1 \right) dz, G_{33}^k = \int_{-h^k/2}^{h^k/2} \frac{1}{4} G l_2^2 \left( \frac{\partial^2 f(z)}{\partial z^2} \right)^2 dz, \\
 G_{44}^k &= \int_{-h^k/2}^{h^k/2} \frac{1}{4} G l_2^2 \left( \frac{\partial f(z)}{\partial z} - 1 \right)^2 dz, O_{66}^k = \int_{-h^k/2}^{h^k/2} f(z) e_{13}^k dz/h^a \\
 Y_{33}^a &= \int_{-h^k/2}^{h^k/2} 2(\pi/h^a) z \xi_{33}^k \sin(\pi z/h^a) dz/h^a, Y_{22}^k = \int_{-h^k/2}^{h^k/2} 2z \xi_{11}^k \cos(\pi z/h^k) dz/h^a \\
 I_i &= \sum_{k=s,t,c,b,a} I_i^k, i = 1,2,3,4, (A_{ij}, C_{ij}, D_{ij}, E_{ij}, F_{ij}, G_{ij}) = \sum_{k=s,t,c,b,a} (A_{ij}^k, C_{ij}^k, D_{ij}^k, E_{ij}^k, F_{ij}^k, G_{ij}^k), i, j = 1,2,3 \\
 (R_{ij}, O_{ij}, S_{ij}) &= \sum_{k=s,a} (R_{ij}^k, O_{ij}^k, S_{ij}^k), i, j = 1,2,3
 \end{aligned}$$